Journal of Medicinal Chemistry

Article

Cite This: J. Med. Chem. 2018, 61, 6140−6152

pubs.acs.org/jmc

Identification of a Potent Tryptophan-Based TRPM8 Antagonist With in Vivo Analgesic Activity

Alessia Bertamino,[†,#] Nunzio Iraci,[†,#] Carmine Ostacolo,[‡,#] Paolo Ambrosino,[§] Simona Musella,[‡] Veronica Di Sarno,[†] Tania Ciaglia,[†] Giacomo Pepe,[†] Marina Sala,[†] Maria Virginia Soldovieri,[§] Ilaria Mosca,[§] Sara Gonzalez-Rodriguez,[∥] Asia Fernandez-Carvajal,[∥] Antonio Ferrer-Montiel,[∥] Ettore Novellino,[‡] Maurizio Taglialatela,[¶] Pietro Campiglia,[*,†] and Isabel Gomez-Monterrey[*,‡]

[†]Department of Pharmacy, University of Salerno, Via G. Paolo II 132, 84084 Fisciano, Salerno Italy

[‡]Department of Pharmacy, University Federico II of Naples, Via D. Montesano 49, 80131 Naples, Italy

[§]Department of Medicine and Health Science V. Tiberio, University of Molise, Via F. de Sanctis, 86100 Campobasso, Italy

[¶]Department of Neuroscience, Reproductive Sciences and Dentistry, University Federico II of Naples, Via Pansini, 5, 80131 Naples, Italy

[∥]Institute of Molecular and Cellular Biology, Universitas Miguel Hernández, Avda de la Universidad, 032020 Elche, Spain

Supporting Information

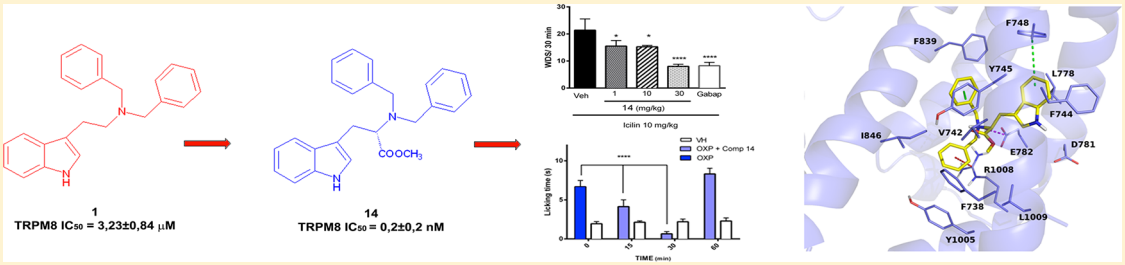

ABSTRACT: TRPM8 has been implicated in nociception and pain and is currently regarded as an attractive target for the pharmacological treatment of neuropathic pain syndromes. A series of analogues of *N*,*N*′-dibenzyl tryptamine **1**, a potent TRPM8 antagonist, was prepared and screened using a fluorescence-based in vitro assay based on menthol-evoked calcium influx in TRPM8 stably transfected HEK293 cells. The tryptophan derivative **14** was identified as a potent (IC_{50} 0.2 ± 0.2 nM) and selective TRPM8 antagonist. In vivo, **14** showed significant target coverage in both an icilin-induced WDS (at 1−30 mg/kg s.c.) and oxaliplatin-induced cold allodynia (at 0.1−1 μg s.c.) mice models. Molecular modeling studies identified the putative binding mode of these antagonists, suggesting that they could influence an interaction network between the S1−4 transmembrane segments and the TRP domains of the channel subunits. The tryptophan moiety provides a new pharmacophoric scaffold for the design of highly potent modulators of TRPM8-mediated pain.

INTRODUCTION

Transient receptor potential melastatin type 8 (TRPM8) channel is a transmembrane Ca^{2+}-permeable nonselective channel[1] triggered by cold temperatures (10−28 °C),[2,3] as well by some specific compounds, such as menthol and icilin, also known as cooling compounds.[2,4] Moreover, TRPM8 is sensitive to transmembrane potential,[5] phosphatidylinositol-4,5-biphosphate (PIP2),[6] and different synthetic molecules.[7−9] TRPM8 channels are widely expressed in different tissues such as skin and mucosae,[10] prostate and bladder,[11] lung epithelium,[12] and artery myocytes.[13] However, the biological significance of TRPM8 in these tissues remains largely undisclosed.

In the last years, a correlation between TRPM8 overexpression and cold allodynia or hyperalgesia has been disclosed in animal models of nerve injury or inflammation.[14,15] Moreover, the typical hyperalgesic response to some types of pain is strongly reduced when TRPM8 antagonists are administered or in TRPM8 knockout mice.[16,17] Upregulation of TRPM8 levels has been also evidenced during the evolution of androgen-sensitive prostate cancer and other malignancies.[18,19]

These findings underscore the high therapeutic potential of these channels in both cancer and pain.[8,20−23] Efforts to identify TRPM8 have strongly increased in the past decade and a wide variety of chemotypes have been recently disclosed as agonists or antagonists.[24,25] Among antagonists, BCTC, a piperazine carboxamide derivative, was shown to inhibit prostate tumor cell growth,[26] while the benzamide-based blocker, AMTB, proved remarkable therapeutic efficacy in animal models of overactive and painful bladder syndromes.[27]

Received: April 6, 2018
Published: June 25, 2018

DOI: 10.1021/acs.jmedchem.8b00545
J. Med. Chem. 2018, 61, 6140−6152

A benzimidazole-based antagonist, identified by a Janssen's research group, demonstrated an excellent inhibitory activity when challenged in animal models of neuropathic pain.[28] Furthermore, researchers from Pfizer identified the isoquinoline derivative PF-05105679, endowed with clinical efficacy in human cold allodynia.[29]

Our research group has recently identified an indole-based derivative [*N*,*N*-dibenzyl-2-(1*H*-indol-3-yl)ethanamine, **1**, Figure 1] inhibiting menthol-induced currents in HEK293 cells

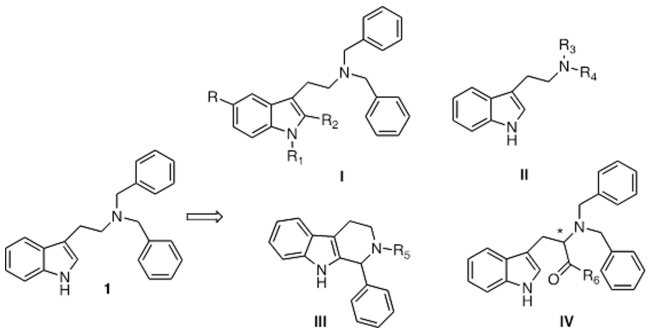

Figure 1. Structure of newly proposed antagonists.

stably expressing TRPM8.[30] In patch-clamp recordings, compound **1** showed concentration-dependent TRPM8 inhibition with higher potency (IC_{50} = 367 ± 24 nM) and selectivity than the reference antagonist BCTC.

Starting from these results, a new small library of indole derivatives was designed, synthesized, and characterized, obtaining new structure−activity relationship (SAR) clues and new potent antagonists of TRPM8 channel with significantly improved potency over the parent compound **1** and potent in vivo antinociceptive activity. Taking advantage of the recently reported cryo-electron microscopy structure of TRPM8,[31] molecular modeling studies provided some clues about the binding mode of the new TRPM8 antagonists being herein described.

RESULTS AND DISCUSSION

Design and Chemistry. For the design of the new TRPM8 antagonist library, we opted to retain the tryptamine scaffold, which allows efficient and extensive structural modifications.

The indole moiety was substituted at N-1, C-2, and C-5 (I, Figure 1), while the benzyl rings on the amine group were decorated or substituted (II). The conformational architecture of the parent compound **1** was also altered by the introduction of constraints on the indole moiety (III) or on the dibenzyl group (II) or replacing the tryptamine template with tryptophan (IV).

New tryptamine derivatives **2**−**4** were synthesized as depicted in Scheme 1. Compounds **1** and **2** were obtained by a double nucleophilic substitution of tryptamine or 5-benzyloxytryptamine with a large excess of benzyl bromide in DCM, using DIPEA as base.[30] N-1 methylation of **1** with CH_3I or addition of 2,4-dinitrobenzenesulphenyl chloride at C-2 in acid media yielded derivatives **3** and **4**, respectively.

Reductive amination of benzaldehyde with tryptamine using sodium borohydride in dry methanol yielded linear compound **5**, while the same reaction in acidic media led to racemic tetrahydro-beta-carboline **6** (Scheme 2). Final compounds **7**, **8**, and **9**−**11** were synthesized via palladium-catalyzed

Scheme 1. Synthesis of Dibenzyl Tryptamine Derivatives 1−4

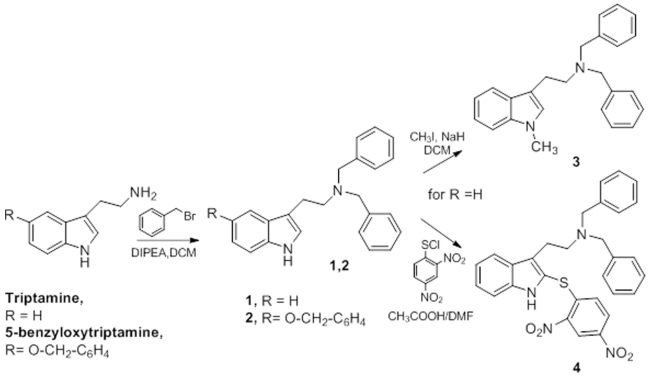

Scheme 2. Synthesis of *N*,*N*-Disubstituted Tryptamine Derivatives (7, 8) and 2-Substituted-1-phenyl-2,3,4,9-tetrahydro-1*H*-pyrido[3,4-*b*]indole (9−11)

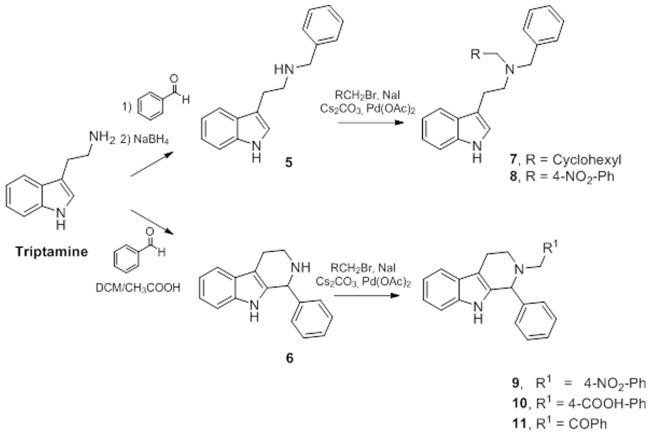

alkylation of the intermediates **5** or **6**, respectively, with the corresponding alkyl, phenylalkyl, or phenacyl bromides. Compounds **9**−**11** were tested as racemic mixtures since all attempts to resolve these mixtures, or the starting beta carboline mixture **6**, by chiral semipreparative HPLC, failed.

Nucleophilic displacement of the 3-(2-bromoethyl)indole by the commercially available 2,3-dihydro-1*H*-benzo[*d*,*e*]-isoquinoline (**12**) led to the restricted analogue **13** (Scheme 3). The synthesis of compounds **14**−**16** was performed starting from L- or D-tryptophan methyl ester, using the same procedure described for derivative **1**. Finally, alkaline hydrolysis of compound **14** gave the acid derivative **15**.

Pharmacological Screening by Ca^{2+}-Imaging Experiments. The activity of the synthesized compounds as TRPM8 blockers was tested in vitro by evaluating their ability to counteract a menthol-induced increase in intracellular Ca^{2+} levels in Ca^{2+} fluorimetric assays in HEK293 cells stably expressing the rat isoform of TRPM8 channels. As reported in Table 1, eight of the 12 compounds synthesized proved to be more potent than the specific antagonist *N*-(3-aminopropyl)-2-[(3-methylpheny)methoxy]-*N*-(2-thienylmethyl) benzamide hydrochloride (AMTB), used as reference compound.

The functionalization at the positions 5 and 2 of the indole ring is well tolerated, and the compounds **2** and **4** weakly improve the potency over compound **1**.

The methylation at the indole N-1 of compound **3** slightly decreased the activity respect to analogues **2** and **4**, although

DOI: 10.1021/acs.jmedchem.8b00545
J. Med. Chem. 2018, 61, 6140−6152

Scheme 3. Synthesis of 1-(2-(1*H*-Indol-3-yl)ethyl)-2,3-dihydro-1*H*-benzo[*d*,*e*]quinoline (13) and L- and D-Tryptophan Derivatives (14−16)

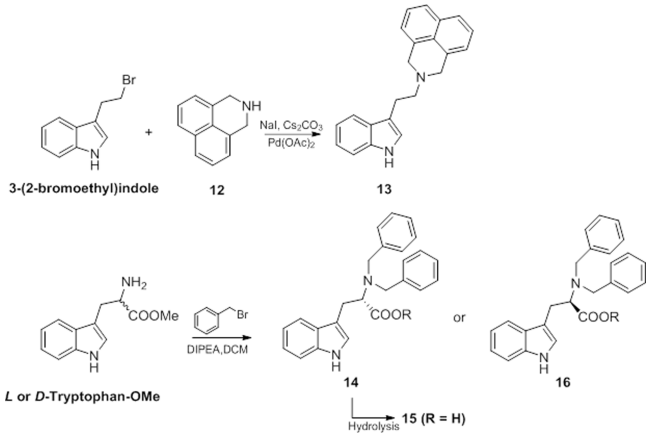

Table 1. Potency of Synthesized Compounds as TRPM8 Antagonists[a]

compound	IC_{50} (μM)
1	3.2 ± 0.8
2	1.9 ± 0.9
3	3.3 ± 1.3
4	2.2 ± 0.7
7	0.6 ± 0.5
8	3.00 ± 0.9
9	3.3 ± 1.3
10	>100
11	1.6 ± 0.9
13	11.8 ± 2.2
14	0.04 ± 0.09
15	8.2 ± 2.1
AMTB	6.5 ± 1.4

[a]Values are expressed as the mean ± standard deviation of three independent measurements.

maintaining the potency in comparison to **1**. Compound **7**, containing a methyl cyclohexyl, in place of a benzyl, group, proved to be 5-fold more effective and potent than **1** (IC_{50} 0.6 ± 0.5 μM versus 3.2 ± 0.8 μM), while the introduction of a strong electron-withdrawing group, such as NO_2, at position 4 in one of the aryl moieties (**8**), maintained the antagonist potency in the micromolar range. Interestingly, the tetrahydro-β-carboline **9** as a restricted analog of **8** still shows micromolar activity, while the replacement of the NO_2 group with a COOH one at the same position (derivative **10**) caused the loss of the antagonist activity. The substitution at N-2 of the benzyl moiety by the more hydrophobic acetophenone group (compound **11**) allowed to recover and even increase the antagonistic potency. However, the conformational restriction introduced using the bulky 2,3-dihydro-1*H*-benzoisoquinoline substituent proved to be deleterious for the activity. Thus, compound **13** resulted 4 times less active than **1**.

Finally, the replacement of tryptamine with the tryptophan scaffold led to the most interesting derivatives. Dibenzyl tryptophan **14**, showing nanomolar potency, is indeed the most potent TRPM8 blocker reported so far. It is interesting to note that the acid derivative **15** resulted 200 times less potent than **14**. We wondered whether this behavior was mainly a matter of pharmacodynamic or pharmacokinetic properties; thus, we challenged the membrane crossing properties of the two compounds by using the Parallel Artificial Membrane Permeability Assay (PAMPA, Figure S1). We found that the ester derivative **14** (Papp = 0.97 ± 0.21 × 10^{-6} cm/s, $QPlogP_{O/W}$ = 5.4) was less prone to cross membranes than **15** (Papp = 3.17 ± 0.81 × 10^{-6} cm/s, $QPlogP_{O/W}$ = 2.9, Figure S1). Thus, it is plausible that the dramatic decrease in activity is mainly due to the pharmacodynamic properties of the investigated molecules. The selectivity of the most potent TRPM8 modulators (**7** and **14**) over TRPV1 was also investigated by calcium fluorimetric experiments in SH-SY5Y cells stably expressing mouse TRPV1 channels, using the prototypical TRPV1 agonist (capsaicin, 10 μM) or antagonist (ruthenium red, 10 μM) as controls. Both compounds displayed high selectivity for TRPM8 channels, showing no activity on TRPV1 (SI, Figure S2).

Pharmacological Properties of Compounds 7, 14, and 16 by Patch-Clamp Electrophysiology. As described, **7** and **14** derivatives were identified as the most potent TRPM8 antagonists by a multicellular Ca^{2+} fluorimetric assay. To further characterize such pharmacological activity in a single cell-based electrophysiological assay, we tested the ability of these compounds to counteract menthol-evoked responses in HEK293 cells transiently expressing rTRPM8 by patch-clamp recordings. Application of menthol (500 μM) resulted in a large, strongly outwardly rectifying current ($I_{+80\ mV}/I_{-80\ mV}$ = 94 ± 19; n = 66) that reverted near to 0 mV (−1.1 ± 0.4 mV; n = 66), consistent with the well-known poor selectivity of rTRPM8 among monovalent cations[1] (Figure 3A). As previously reported,[30] menthol EC_{50} was 75 ± 4 μM, a value consistent with that shown for rTRPM8 when expressed in *Xenopus* oocytes (67 μM).[1] The nontransfected cells were insensitive to menthol (data not shown), confirming that menthol-activated currents were strictly dependent on the expression of rTRPM8. As also shown in the time-course experiments of Figure 2A,B (left panels), 500 μM menthol-evoked rTRPM8 currents were rather stable for at least 1 min; during menthol exposure, addition of 500 nM **7** (Figure 2A) or 100 nM **14** (Figure 2B) almost fully blocked menthol-gated rTRPM8 currents, thus showing potent antagonistic properties. The inhibitory effects of both **7** and **14** were fully reversible, as menthol-evoked currents were largely recovered upon washout of the drugs. The inhibitory effects of both **7** and **14** compounds on menthol-evoked rTRPM8 currents were concentration-dependent (Figure 2C, left panel), showing IC_{50}s of 3.5 ± 0.6 nM (n = 28) and 0.2 ± 0.2 nM (n = 16), respectively (Figure 2C, right panel); these values are well below those reported for the canonical TRPM8 antagonist BCTC (IC_{50} = 475 nM)[31] as well as for the reference compound **1** (IC_{50} = 367 nM).[30] Noteworthy, comparison of the absolute IC_{50} values calculated from intracellular Ca^{2+} and electrophysiological assays for both compounds **7** and **14** confirmed the rank order of potency for these compounds, with **14** being more potent than **7**.

To determine the role of the chiral center in the rTRPM8-blocking activity of compound **14**, the pharmacological effects of its D-enantiomer **16** was also investigated. As shown in Figure 2C, **16** showed a similar efficacy but a >4000-times reduced potency (IC_{50} = 865 ± 26 nM; n = 20) when compared to the L-enantiomer **14**, therefore suggesting a crucial role played by the chiral center in the pharmacological properties shown by compound **14**.

DOI: 10.1021/acs.jmedchem.8b00545
J. Med. Chem. 2018, 61, 6140−6152

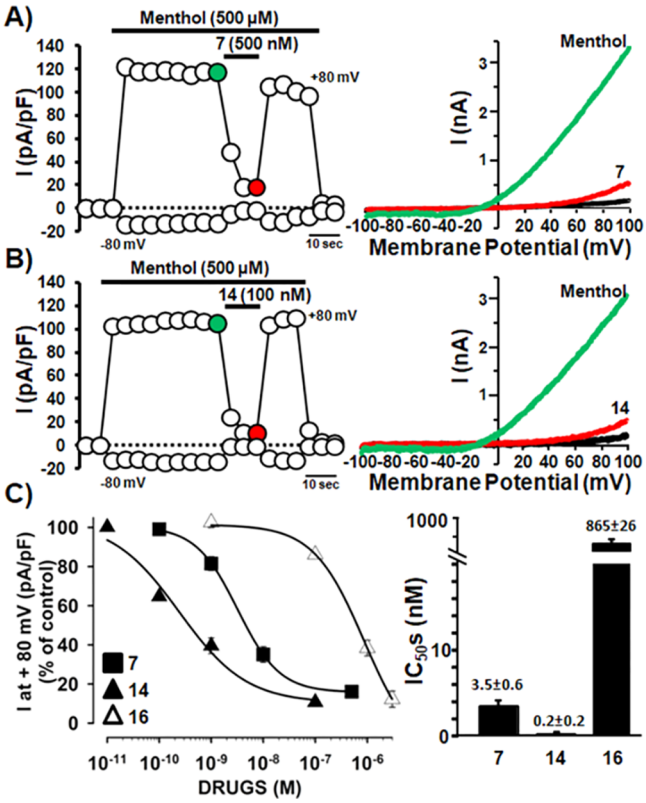

Figure 2. Compounds **7** and **14** block menthol-evoked TRPM8 currents in HEK293 cells. (A,B left) Time-course of currents recorded at +80 or −80 mV in HEK293 cells transiently expressing TRPM8 upon application of 500 μM menthol + derivative **7** (500 nM, A) or 500 μM menthol + derivative **14** (100 nM, B). (A,B right) Representative current traces from a single TRPM8-transfected HEK293 cell subsequently exposed to control solution (CTL, black trace), 500 μM menthol (green traces), and 500 μM menthol + 500 nM derivative **7** (red trace; A) or 500 μM menthol + 100 nM derivative **14** (red trace; B). Traces shown are those indicated in each respective color (black, green, red) in the time-course shown in the left panels. (C) Dose−response curve for **7**-, **14**-, and **16**-induced inhibition of TRPM8 currents (left panel), and resulting IC_{50} for each compound (right panel).

Molecular Modeling and Structural Rationale. In order to rationalize the SAR of **1** and other analogues, we previously built a model of TRPM8 bound to compound **1**,[31] based on the homology model by Taberner et al.,[32] which highlighted the pivotal role of the linker between S6 and TRP box (amino acids 980−992 in rat TRPM8) for the channel gating. In particular, we used a simplified version of the model and proposed that our antagonists docked at a putative binding site in the VSLD cavity. This putative binding region is supposed to bind diverse chemotypes, such as β-lactam derivatives,[33] naphtyl derivatives,[34] tetrahydroisoquinolines, and 2,5-diketopiperazines.[35] In this work, we created a new model of human TRPM8 using the recently published *ficedula albicollis* TRPM8 ($TRPM8_{FA}$) structure as template. The $TRPM8_{FA}$ experimental model shows significant differences with respect to TRPV1, TRPV2, and previously reported TRPM8 models, and redefines the location of several residues involved in modulator binding.[31]

Focusing on the region formed by TM helices S1−6 and TRP box (residues 723−1013), we modeled a human TRPM8 monomer by homology with $TRPM8_{FA}$, using the Prime software.[36]

It is worth noting that $TRPM8_{FA}$ shows a high similarity with human TRPM8, and this similarity gets higher when focusing on the binding region delimited by TM helices S1−6 and the TRP box (Table S1).

In the resulting model, the VSLD region appears almost divided into two layers, with a very hydrophobic top one and a bottom one populated by charged residues interacting mutually. In particular, R1008 interacts with E1004, D781, and E782, while R842 interacts with D802 and E782. R784 points instead outside of the VSLD cavity (Figure 3A).

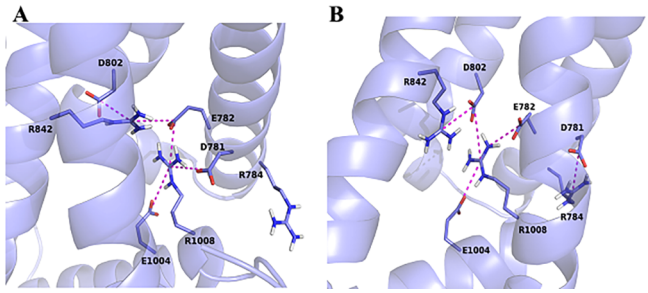

Figure 3. Ionic interactions (represented as magenta dashed lines) between charged residues of the VSLD cavity in the apo protein (A) and upon binding of compound **1** (B).

We performed an Induced Fit Docking (IFD)[37,38] simulation of compound **1** on the homology model and submitted the best scoring **1**/TRPM8 complex to a 48 ns long molecular dynamics simulation.

The simulations showed the indole NH interacting with Asp781, and the nitrogen of the linker with Glu782. One of the two phenyl rings can engage cation−π interactions with arginines 842 and 1008. Residues Y1005, F839, and F744 can make π−π interactions with the three rings of the antagonist. Further interactions, mainly hydrophobic, are observed with residues F738, Y745, L778, I846, and L1009 (Figure 4).

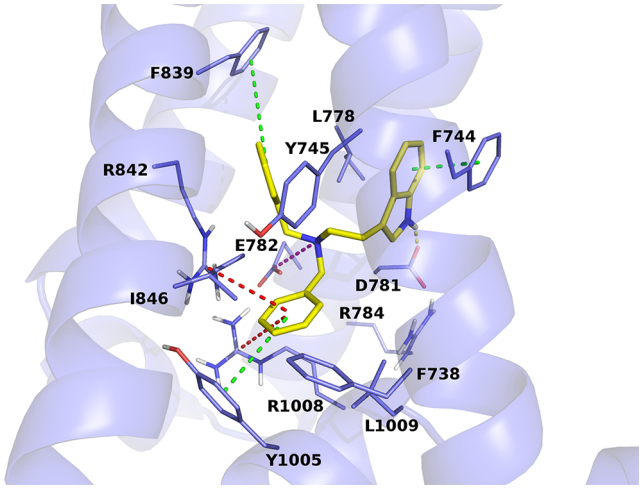

Figure 4. Bound conformation of compound **1**, depicted as yellow sticks. TRPM8 is depicted as blue cartoons and sticks. Dashed lines represent π−π, π−cation, salt bridge, and H-bond interactions between TRPM8 and compound **1**, and are color-coded in green, red, magenta, and yellow, respectively.

DOI: 10.1021/acs.jmedchem.8b00545
J. Med. Chem. 2018, 61, 6140−6152

It is interesting to note how the architecture of the ionic interactions described above for the unbound protein changes upon binding of **1** (Figure 3B). Indeed, D781, which previously interacted with R1008, now moves away from the cavity and interacts with R784. R1008 continues to interact with E782 but establishes two new interactions with F802 and with the phenyl ring of the ligand. R842 no longer interacts with E782 but continues to interact with D802 and establishes a new interaction with one of the phenyl rings of the ligand. It seems that the addition of the positive charge of the ligand and the displacement of D781 tend to neutralize the negative charge of the pocket, and this could stabilize an inactive conformation of the channel.

We used the predicted **1**/TRPM8 complex, after MD equilibration (see materials and methods), as target for constrained molecular docking simulations of compounds **2**−**4**, **7**−**11**, and **13**−**16** (Figure S2a-i), using the Glide program.[39]

Docking of compound **3** (Figure S3a) shows a deviation of the indole moiety caused by the methylation of NH and a loss of the interaction with D781. Since the compound still shows a good activity we suggest that despite this interaction could increase the activity, its lack does not substantially compromise it.

Modifications at position 5 and 2 of the indole ring are well tolerated. The accommodation of the benzyl ether group in **2** (Figure S3b), near to the residues L778, L774, L806, F839, and F748, slightly improves the activity of the product with respect to **1**, whereas the additional phenyl sulfane of **4** (Figure S3c) points toward the membrane and does not influence the activity.

The cyclohexyl group of compound **7** (Figure S3d), which is docked in the hydrophobic region of the site surrounded by residues L778, L806, F748, L774, F839, and Y745, leads to a 5-fold activity improvement suggesting that in this binding region a hydrophobic and aliphatic moiety may interact stronger than an aromatic one.

Compounds **8** and its more conformational restricted analogue **9** address the nitro group in different directions (Figure S3e,f), showing that it could probably be tolerated in two different areas of the pocket. The restrained strengthening of the **9** scaffold prevents NH indole from interacting with D781 showing, once again, that this interaction is not necessary for the activity.

Substitution of the nitro group of **9** with a carboxyl one, as in compound **10** (Figure S3g), leads to a dramatic loss of activity; bound conformations of **9** and **10** show the nitro and carboxyl groups docked in the same area. Although these compounds have been tested as racemic mixtures, our modeling study indicates that the *R* enantiomer is the most active in this tetrahydro-carboline series as confirmed even by the most potent compound **11** (Figure S3h), whose 4-substituted benzyl is replaced by a $-CH_2-$benzoyl group.

Docking of compound **13** (Figure S3i), highlights the lack of any potential cation−π interaction at the level of R1008, revealing a potential mechanism for its decreased potency when compared to compound **14** (see below). It is, however, important to note that the binding mode of this compound suggests that the hydrophobic "roof" area could accommodate, besides phenyl groups or aliphatic substituents as in compound **7**, even larger substituents.

Dibenzyl tryptophan derivative **14**, indeed the most potent TRPM8 inhibitor reported so far, with an IC_{50} in the subnanomolar range (0.2 nM, see Figure 2C), shares most of its interactions with the parent compound **1**. The **14**/TRPM8 complex, during a 48 ns long molecular dynamics simulation, reveals an interaction with Y745, which is reported as a critical residue for the binding of menthol and SKF963635.[40] The interaction with E781 is weaker than **1**, and this confirms once again that this hydrogen bond is not fundamental for the activity of the antagonists (Figure 5). The additional carboxymethyl group docks in a hydrophobic area surrounded by residues V742, I846, L1009, N741, and Y745.

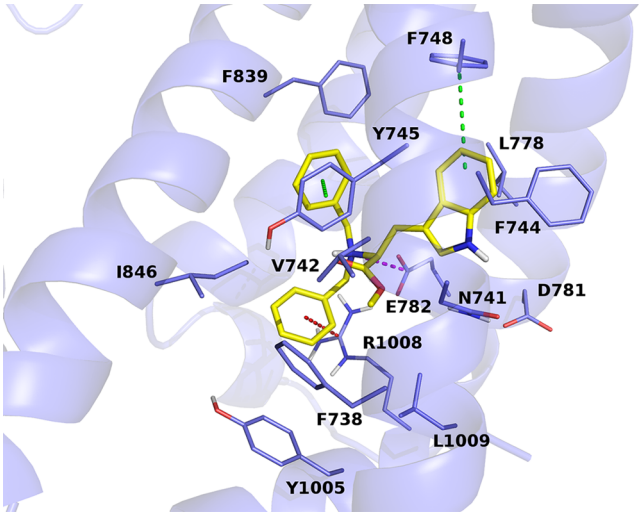

Figure 5. Bound conformation of compound **14**, depicted as yellow sticks. TRPM8 is depicted as blue cartoons and sticks. Dashed lines represent $\pi-\pi$, π−cation, and salt bridge interactions between TRPM8 and compound **14** and are color-coded in green, red, and magenta, respectively.

This feature, together with the negative net charge of the site, could explain the dramatic loss of activity showed by its acid derivative **15**. The inversion of chiral configuration as in compound **16**, projects the carboxymethyl group to an area surrounded by R1008, E782, L778, and D781 (Figure 6), and the proximity of charged residues could contribute to the loss of activity shown by the **16** enantiomer.

Our molecular modeling studies highlight the plausible importance of several VSLD cavity residues in the binding of TRPM8 modulators. Indeed, charged residues like D781, E782, R784, D802, R842, E1004, and R1008 could be likely involved in the equilibrium between functional states of the channel, and our docking simulations show the interaction of these residues with our indole derivatives. In particular, E782, R842, and R1008 are always predicted to be involved in ionic and $\pi-\pi$ stacking interactions with our inhibitors. If, on one side, the above-mentioned charged residues may look like the most important VSLD residues in the gating mechanism, several others may be responsible for an efficient inhibitor binding. The interaction with hydrophobic residues V742, L778, L806, I846, F748, L774, F839, Y745, V742, and L1009 appears indeed desirable for an efficient antagonist activity. Overall, using a simplified channel model, our molecular studies gave some clues about the gating and modulation mechanisms of TRPM8 that need to be challenged through further in-depth experimental and computational studies.

In Vivo Pharmacological Characterization of Compound 14. *Wet-Dog Shakes Assay.* To determine whether

DOI: 10.1021/acs.jmedchem.8b00545
J. Med. Chem. 2018, 61, 6140−6152

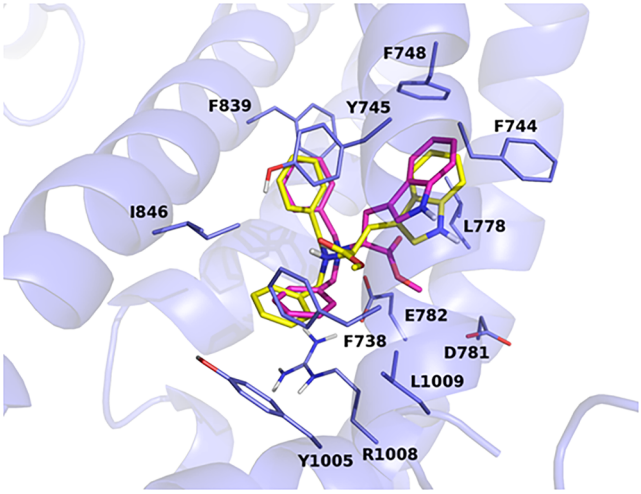

Figure 6. Bound conformation of compound **16**, depicted as magenta sticks. TRPM8 is depicted as blue cartoons and sticks. Compound **14** is represented as yellow sticks for reference.

the observed in vitro TRPM8 inhibitory activity of compound **14** also translates in TRPM8-dependent antinociceptive activity in vivo, a "wet-dog shakes" (WDS) assay was performed.[41] In this assay, the potent TRPM8 agonist icilin (10 mg/kg intraperitoneally i.p.), was injected in mice treated with **14** or vehicle. Mouse TRPM8 is known to share high homology with rat TRPM8, which has been used for in vitro assays.[30] Icilin injections in mice produce vivid and quantifiable TRPM8-mediated shaking behaviors.[28,42] The compound **14** (1, 10, and 30 mg/kg) or its vehicle were administered subcutaneously (s.c.) 30 min before icilin injection. As shown in Figure 7, compound **14** produced a marked, dose-dependent

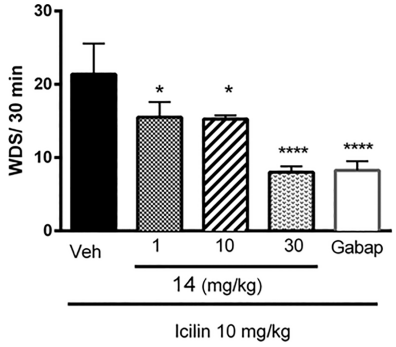

Figure 7. Effect of **14** on icilin-induced WDS in C57BL/6J mice. Compound **14** or vehicle was administered 30 min before icilin injection. Gabapentin was administered 1 h before icilin injection. After i.p. injection of icilin (10 mg/kg), the number of wet-dog shakes (WDS) were counted over 30 min. Data are given as mean ± SEM (n = 6). Two-way ANOVA with Bonferroni post hoc test. *P < 0.05; **P < 0.01, ***P < 0.001,**** P < 0.001.

antinociceptive behavior; at the highest dose of 30 mg/kg, **14** inhibited WDS-like cold hypersensitivity in mice by 63%, thus showing an efficacy comparable to that observed with a standard analgesic dose of gabapentin (25 mg/kg, s.c.)

Cold Allodynia. As indicated in the introduction, increasing evidence suggest that TRPM8 plays a critical role in mouse models of chemotherapy-induced neuropathic pain evoked by oxaliplatin (OXP), a condition mimicking cold hypersensitivity provoked by chemotherapy-induced peripheral neuropathy (CIPN).[43] In fact, acute and chronic OXP-induced cold hypersensitivity have been reproduced in rats and mice and correlated with TRPM8 expression and function.[44,45] The TRPM8 agonist menthol has shown antiallodynic activity in a neuropathic rat model,[46] and its topical administration showed analgesic efficacy in human chemotherapy-induced neuropatic pain.[47] However, it has been reported that, in a rodent model, acute cold allodynia after OXP injection was alleviated by the TRPM8 blockers *N*-(2-aminoethyl)-*N*-[4-(benzyloxy)-3-methoxybenzyl]-*N*′-(1S)-1-(phenyl) ethyl] urea and TC-I 2014.[48] According to these findings we investigated the effect of our antagonist **14** in an OXP-induced cold allodynia model, using acetone for cooling stimulation. Considering that cold pain threshold is increased from ∼12 °C to ∼26 °C in OXP-treated patients, acetone stimulation is considered to evoke pain in OXP-treated mice.[48]

The activity of compound **14** was evaluated at day 7 after intraperitoneal administration of three OXP doses (6 mg/kg) in C57/BL6 mice, when cold allodynia had developed. After single subcutaneous administration of **14** (0.1 and 1 μg), attenuated cold allodynia was evident at 15 min and reaches the maximum inhibition 30 min after administration (Figure 8A,B) in a dose-dependent manner.

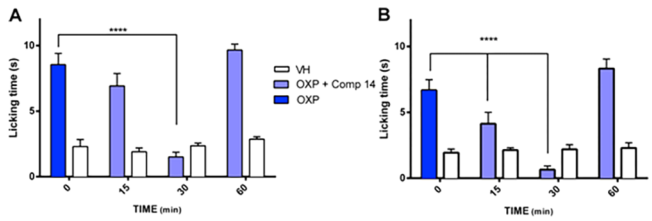

Figure 8. Oxaliplatin (OXP)-induced cold allodynia and effects of TRPM8 blocker (**14**). Mice were given three i.p. injections of OXP (6 mg/kg) or the vehicle (VH) on alternate days. Cold allodynia was evaluated by the acetone test. Time-course of cold allodynia after OXP injection. Effects of the TRPM8 blocker at 0.1 (A) or 1.0 μg (B). Data are given as mean ± SEM (n = 6). Two-way ANOVA with Bonferroni post hoc test. *P < 0.05; **P < 0.01, ***P < 0.001.

Although highly potent, compound **14** showed a short lasting effect in both the animal models used. We argued that this effect could be due to the presence of the labile ester moiety, readily prone to generate the less active acid derivative **15**. This hypothesis was challenged by enzymatic stability assay in mice serum and chemical stability assay in phosphate buffer. The compound resulted stable to chemical hydrolysis when dissolved in phosphate buffer at pH 7.4 for 1 h (Figure S4). Contrariwise, **14** is almost completely metabolized during a 1 h time course experiment in mice serum, generating **15** as the major metabolite (Figures S4 and S5). It must be considered that the high potency of derivative **14** could also be justified on the basis of a multitargeted activity. Many different ionotropic and metabotropic receptors[43,44] have been described to mediate oxaliplatin-induced neuropathy. Among these, the TRPA1 receptors, located also on primary afferent neurons, is involved in mechanical and cold allodynia.[49] Recently, Pan et al.[50] described that TRPA1 and TRPM8 promote a local vasodilatation that aggravate the oxaliplatin-induced peripheral neuropathy and that blockade of TRPA1 and/or TRPM8 receptors attenuated this process. According to these results a "double block" of TRPM8 and TRPA1 could represent a potential pharmacological advantage. To address this hypoth-

DOI: 10.1021/acs.jmedchem.8b00545
J. Med. Chem. 2018, 61, 6140−6152

esis, studies on TRPA1 activity with different tryptophan derivatives are ongoing.

CONCLUSIONS

In this work, the synthesis and the pharmacological characterization of a small library of TRPM8 antagonists have been reported. One of the synthesized derivatives, compound **14**, proved to be the most potent in vitro TRPM8 antagonist identified so far, producing a selective and complete TRPM8 inhibition with potency in the subnanomolar range. In vivo studies showed that compound **14** suppresses TRPM8-mediated cold hypersensitivity and significantly reduces cold allodynia in vivo. According to these findings, **14** represents a new lead compound and a new pharmacological tool to investigate TRPM8-mediated signaling. Moreover, a new TRPM8 homology model has been built, allowing to hypothesize a binding mode for this series of TRPM8 modulators, to rationalize their pharmacological activity and to provide useful findings for the rational development of new TRPM8 blockers.

EXPERIMENTAL SECTION

General. Reagents, starting materials, and solvents were purchased from Sigma-Aldrich (Milan, Italy) and used as received. Reactions were carried out with magnetic stirring in round-bottomed flasks unless otherwise noted. Moisture-sensitive reactions were conducted in oven-dried glassware under a positive pressure of dry nitrogen, using predried, freshly distilled solvents. Microwave-assisted reactions were performed in a Biotage Initiator+ reactor. Analytical thin layer chromatography (TLC) was performed on precoated glass silica gel plates 60 (F254, 0.25 mm, VWR International). Purifications were performed by flash column chromatography on silica gel (230−400 mesh, Merck Millipore). One- and two-dimensional NMR spectra were recorded with a Bruker Avance (400 MHz) spectrometer, at room temperature. Spectra were referenced to residual chloroform (7.24 ppm, ^{1}H; 77.23 ppm, ^{13}C) or methanol (3.31 ppm, ^{1}H; 49.15 ppm, ^{13}C). Chemical shifts are reported in δ values (ppm) relative to internal Me_4Si, and J values are reported in hertz (Hz). The following abbreviations are used to describe peaks: s (singlet), d (doublet), dd (double doublet), t (triplet), q (quartet), and m (multiplet). HR-MS experiments were performed using an LTQ-Orbitrap-XL-ETD mass spectrometer (Thermo Scientific, Bremen, Germany), using electrospray ionization. Optical rotations were measured on an Atago Polax 2-L polarimeter, at the concentration of 0.1 g/100 mL. Analytical RP-HPLC was performed on a Phenomenex Synergi Fusion RP-80A (75 mm × 4.6 mm, 4 μm), with a flow rate of 1 mL/min, using a tunable UV detector at 254 nm. Mixtures of CH_3CN and 0.05% TFA in H_2O were used as mobile phase. All compounds showed a purity ≥95%.

*Synthesis of N,N-Dibenzyl-2-(5-(benzyloxy)-1H-indol-3-yl)-ethanamine (**2**).* Obtained according to the synthetic procedure previously described.[30] Colorless oil (71% yield). ^{1}H NMR (400 MHz, $CDCl_3$) δ 2.83 (t, 2H, CH_2 J = 8.4 Hz); 2.98 (t, 2H, CH_2 J = 8.4 Hz); 3.73 (s, 4H, CH_2); 4.97 (s, 2H, CH_2); 6.92 (s, 3H, aryl); 7.23−7.25 (m, 3H, aryl); 7.29−7.38 (m, 5H, aryl); 7.42−7.44 (m, 6H, aryl); 7.51 (d, 2H, aryl, J = 7.6 Hz); 7.80 (s, 1NH); ^{13}C NMR (100 MHz, $CDCl_3$) δ 23.2; 53.8; 58.4; 71.0; 102.2; 111.7; 112.9; 114.4; 122.3; 126.8; 127.7; 127.8; 127.9; 128.2; 128.5; 128.8; 131.6; 137.7; 140.0; 153.1. HR-MS m/z calcd for $C_{31}H_{31}N_2O$ $[(M + H)^+]$: 447.2431; found 447.2439.

*Synthesis of N,N-Dibenzyl-2-(1-methyl-1H-indol-3-yl)-ethanamine (**3**).* *N*,*N*-Dibenzyl-2-(1*H*-indol-3-yl)ethanamine (**1**, 1.0 equiv) was dissolved in a mixture of anhydrous DCM/DMF (2/1 v/v) under magnetic stirring, and the temperature was set to 0 °C. To this solution, 1.2 equiv of NaH were added portionwise, and the mixture was allowed to react for 30 min. Then, 1.2 equiv of methyl iodide in DCM were added dropwise, and the reaction was warmed to room temperature and maintained under stirring for further 12 h. The reaction was quenched by 10% aqueous solution of citric acid and washed with brine. Organic layer was separated, dried over anhydrous Na_2SO_4, filtered, and evaporated in vacuo. Crude products were purified by column chromatography using *n*-hexane/ethyl acetate (4:1 v/v) as mobile phase.

Colorless oil (65% yield). ^{1}H NMR (400 MHz, $CDCl_3$) δ 2.83 (t, 2H, CH_2, J = 8.0 Hz); 3.00 (t, 2H, CH_2, J = 8.0 Hz); 3.72 (s, 7H, CH_2 and CH_3); 6.76 (s, 1H, aryl); 7.05 (t, 1H, aryl, J = 7.6 Hz); 7.21 (t, 1H, aryl, J = 7.2 Hz); 7.27 (d, 3H, aryl, J = 7.6 Hz); 7.34 (t, 3H, aryl, J = 7.2 Hz); 7.39−7.43 (m, 6H, aryl); ^{13}C NMR (100 MHz, $CDCl_3$) δ 23.0; 32.5; 54.2; 58.4; 109.0; 113.0; 118.5; 119.0; 121.4; 126.3; 126.8; 128.2; 128.8; 139.9. HR-MS m/z calcd for $C_{25}H_{27}N_2$ $[(M + H)^+]$: 355.2169; found 355.2177.

*Synthesis of N,N-Dibenzyl-2-(2-((2,4-dinitrophenyl)thio)-1H-indol-3-yl)ethanamine (**4**).* *N*,*N*-Dibenzyl-2-(1*H*-indol-3-yl)-ethanamine[30] (**1**, 1.0 equiv) was dissolved in a mixture of CH_3COOH/DMF (4:1 v/v) under magnetic stirring at room temperature. Then, 2,4-dinitro sulphenyl chloride (2.0 equiv) was added, and the solution was stirred for 2 h. Then, the reaction was quenched by 10% aqueous solution of sodium carbonate and extracted with DCM (3 × 50 mL), and the organic layer was dried over anhydrous Na_2SO_4, filtered, and evaporated in vacuo. Final compound **4** was obtained after flash chromatography using a mixture of ethyl acetate/*n*-hexane (4.8:0.2 v/v) as eluent.

Yellow oil (52% yield). ^{1}H NMR (400 MHz, $CDCl_3$) δ 2.66 (t, 2H, CH_2, J = 8.0 Hz); 3.07 (t, 2H, CH_2, J = 8.0 Hz); 3.71 (s, 4H, CH_2); 6.71 (d, 1H, aryl, J = 12.0 Hz); 7.13−7.25 (m, 7H, aryl); 7.31−7.42 (m, 7H, aryl); 7.93 (d, 1H, aryl, J = 8.2 Hz); 8.08 (s, 1NH); 9.07 (s, 1H, aryl). ^{13}C NMR (100 MHz, $CDCl_3$) δ 22.5; 29.7; 53.3; 58.4; 111.4; 117.6; 120.1; 120.5; 121.5; 124.9; 126.9; 127.0; 127.5; 128.1; 128.6; 137.7; 139.4; 143.8; 144.8. HR-MS m/z calcd for $C_{30}H_{27}N_4O_4S$ $[(M + H)^+]$: 539.1748; found 539.1760.

*Synthesis of Derivatives N-Benzyl-2-(1H-indol-3-yl)ethanamine (**5**).* Tryptamine (1.0 equiv) was dissolved in dry methanol at room temperature under nitrogen atmosphere. To this solution, 1.0 equiv of benzaldehyde was added, and the mixture was reacted for 12 h. Then, 2.0 equiv of sodium borohydride was added portionwise, and the mixture was reacted for further 3 h. Methanol was then evaporated in vacuo, and the mixture was reconstituted in DCM and washed with brine (3 × 50 mL). The organic phase was separated, dried over Na_2SO_4, filtered, and concentrated in vacuo. The crude product was purified by column chromatography using a mixture of DCM/MeOH (4.5/0.5 v/v) as eluent, obtaining intermediate **5** as a colorless oil in 78% yield.

^{1}H NMR (400 MHz, $CDCl_3$) δ 2.87 (t, 2H, CH_2, J = 8.2 Hz); 2.96 (t, 2H, CH_2, J = 8.2 Hz); 4.91 (s, 2H, CH_2); 6.97−7.02 (m, 2H, aryl); 7.09 (t, 1H, aryl, J = 8.0 Hz); 7.20−7.26 (m, 5H, aryl); 7.35 (d, 1H, aryl, J = 8.0 Hz); 7.51 (d, 1H, aryl). HR-MS m/z calcd for $C_{17}H_{19}N_2$ $[(M + H)^+]$: 251.1543; found 251.1549.

*Synthesis of (R,S)-1-Phenyl-2,3,4,9-tetrahydro-1H-pyrido[3,4-b]-indole (**6**).* Tryptamine (1.0 equiv) was dissolved in a solution of DCM/CH_3COOH (4:1 v/v) at room temperature, and benzaldehyde (1.0 equiv) was added. The mixture was stirred for 3 h and then was quenched by 1 N aqueous NaOH. The organic phase was extracted one more time. Then it was dried over Na_2SO_4, filtered, and evaporated. The crude product was purified by column chromatography using a mixture of DCM/MeOH (4.5:0.5 v/v) as eluent, obtaining intermediate **6** as a colorless oil in 82% yield.

^{1}H NMR (400 MHz, $CDCl_3$) δ 2.72−2.79 (m, 1H, CH_2); 2.83−2.91 (m, 1H, CH_2); 3.04−3.11 (m, 1H, CH_2); 3.29−3.34 (m, 1H, CH_2); 5.11 (s, 1H, CH); 7.02−7.09 (m, 2H, aryl); 7.15 (d, 1H, aryl, J = 8.0 Hz); 7.24−7.29 (m, 5H, aryl); 7.43 (s, 1NH); 7.47 (d, 1H, aryl, J = 8.0 Hz). HR-MS m/z calcd for $C_{17}H_{17}N_2$ $[(M + H)^+]$: 249.1386; found 249.1395.

*General Procedure for the Synthesis of Derivatives **7** and **8**.* Compound **5** (1.0 equiv) was dissolved in acetone, and NaI (0.8 equiv), Cs_2CO_3 (2.0 equiv), and $Pd(OAc)_2$ (0.01 equiv) were added together with the proper alkyl or aryl bromide (0.8 equiv). The reaction was refluxed for 12 h. The resulting mixture was filtered through Celite, dried in vacuo, and reconstituted in DCM. The

DOI: 10.1021/acs.jmedchem.8b00545
J. Med. Chem. 2018, 61, 6140−6152

organic phase was washed with water (3 × 50 mL), dried over anhydrous Na_2SO_4, filtered, concentrated, and purified by column chromatography using ethyl acetate/*n*-hexane as mobile phase.

*N-Benzyl-N-(cyclohexylmethyl)-2-(1H-indol-3-yl)ethanamine (**7**).* Colorless oil (39% yield). ^{1}H NMR (400 MHz, $CDCl_3$) δ 0.69−0.78 (m, 2H, CH_2); 1.03−1.13 (m, 3H, CH_2); 1.40−1.47 (m, 1H, CH); 1.58−1.62 (m, 3H, CH_2); 1.73−1.77 (m, 2H, CH_2); 2.24 (d, 2H, CH_2, J = 8.0 Hz); 2.67 (t, 2H, CH_2, J = 8.2 Hz); 2.84 (t, 2H, CH_2, J = 8.2 Hz); 3.58 (s, 2H, CH_2); 6.87 (s, 1H, aryl); 6.99 (t, 1H, aryl, J = 8.0 Hz); 7.08 (t, 1H, aryl, J = 8.0 Hz); 7.15 (t, 1H, aryl, J = 8.0 Hz); 7.22 (t, 3H, aryl, J = 8.0 Hz); 7.28 (t, 2H, aryl, J = 8.0 Hz); 7.40 (d, 1H, aryl, J = 8.0 Hz); 7.79 (s, 1NH); ^{13}C NMR (100 MHz, $CDCl_3$) δ 23.1; 26.2; 26.9; 31.9; 36.2; 54.8; 59.4; 61.4; 111.0; 115.0; 118.9; 119.1; 121.4; 121.8; 126.6; 127.6; 128.0; 128.8; 136.2; 140.5. HR-MS m/z calcd for $C_{24}H_{31}N_2$ [$(M + H)^+$]: 347.2482; found 347.2490.

*N-Benzyl-2-(1H-indol-3-yl)-N-(4-nitrobenzyl)ethanamine (**8**).* Yellow oil (53% yield). ^{1}H NMR (400 MHz, $CDCl_3$) δ 2.85 (t, 2H, CH_2, J = 7.2 Hz); 3.01 (t, 2H, CH_2, J = 7.2 Hz); 3.74 (s, 2H, CH_2); 3.76 (s, 2H, CH_2); 6.94 (s, 1H, aryl); 7.04 (t, 1H, aryl, J = 8.0 Hz); 7.19 (t, 1H, aryl, J = 8.0 Hz); 7.30−7.47 (m, 9H, aryl); 7.94 (s, 1NH); 8.08 (d, 2H, aryl, J = 8.8 Hz); ^{13}C NMR (100 MHz, $CDCl_3$) δ 23.3; 54.3; 57.8; 58.6; 111.1; 114.3; 118.7; 119.2; 121.5; 122.0; 123.3; 127.1; 127.4; 128.4; 128.8; 129.1; 136.2; 139.2; 146.9; 148.1. HR-MS m/z calcd for $C_{24}H_{24}N_3O_2$ [$(M + H)^+$]: 386.1863; found 386.1869.

*General Procedure for the Synthesis of Derivatives **9**−**11**.* Final compounds **9**−**11** were obtained by reaction of intermediate **6** with the proper alkyl or aryl bromide in the same conditions described for compounds **7** and **8**.

*(R,S)-2-(4-Nitrobenzyl)-1-phenyl-2,3,4,9-tetrahydro-1H-pyrido-[3,4-b]indole (**9**).* Yellow oil (48% yield). ^{1}H NMR (400 MHz, $CDCl_3$) δ 2.73 (dd, 1H, H-4′, J' = 6.0, J'' = 1.8 Hz); 2.78 (d, 1H, H-4″, J = 7.8 Hz); 2.86−3.02 (m, 1H, H-3′); 3.16 (dd, 1H, H-3″, J' = 1.8, J'' = 16.0 Hz); 3.51 (d, 1H, CH_2 benzyl, J = 16.0 Hz); 3.98 (d, 1H, CH_2 benzyl, J = 16.0 Hz); 4.71 (s, 1H, H-1); 7.11−7.17 (m, 2H, aryl); 7.22 (d, 1H, aryl, J = 8.0 Hz); 7.29 (s, 1NH); 7.35−7.43 (m, 3H, aryl); 7.47 (d, 2H, aryl, J = 8.4 Hz); 7.55 (d, 3H, aryl, J = 8.0 Hz); 8.20 (d, 2H, aryl, J = 8.0 Hz); ^{13}C NMR (100 MHz, $CDCl_3$) δ 21.3; 48.9; 57.8; 65.1; 108.8; 110.8; 118.3; 119.5; 121.7; 123.5; 127.1; 128.4; 134.4; 136.3; 140.9; 147.1; 147.7. HR-MS m/z calcd for $C_{24}H_{22}N_3O_2$ [$(M + H)^+$]: 384.1707; found 384.1715.

*(R,S)-4-((1-Phenyl-3,4-dihydro-1H-pyrido[3,4-b]indol-2(9H)-yl)-methyl)benzoic Acid (**10**).* White solid (45% yield). ^{1}H NMR (400 MHz, DMSO) δ 2.63−2.71 (m, 1H, H-4′); 2.75−2.82 (m, 2H, H-3); 2.98−3.03 (m, 1H, H-4″); 3.61 (d, 1H, CH_2 benzyl, J = 12.0 Hz); 3.78 (d, 1H, CH_2 benzyl, J = 12.6 Hz); 4.77 (s, 1H, H-1); 6.96 (t, 1H, aryl, J = 7.8 Hz); 7.01 (t, 1H, aryl, J = 7.8 Hz); 7.23 (d, 1H, aryl, J = 7.8 Hz); 7.29−7.37 (m, 5H, aryl); 7.43 (d, 1H, aryl, J = 8.0 Hz); 7.47 (d, 2H, aryl, J = 7.8 Hz); 7.92 (d, 2H, aryl, J = 8.0 Hz); 10.35 (s, 1NH). ^{13}C NMR (100 MHz, DMSO) δ 20.6; 46.9; 49.1; 57.4; 63.1; 107.5; 111.6; 118.1; 118.8; 121.1; 126.9; 128.0; 128.7; 129.3; 129.8; 130.0; 134.9; 136.8; 142.1; 145.3; 167.7. HR-MS m/z calcd for $C_{25}H_{23}N_2O_2$ [$(M + H)^+$]: 383.1754; found 383.1761.

*(R,S)-1-Phenyl-2-(1-phenyl-3,4-dihydro-1H-pyrido[3,4-b]indol-2(9H)-yl)ethanone (**11**).* Colorless oil (60% yield). ^{1}H NMR (400 MHz, $CDCl_3$) δ 2.87−2.92 (m, 1H, H-4′); 2.98−3.03 (m, 1H, H-4″); 3.06−3.11 (m, 1H, H-3′); 3.27−3.31 (m, 1H, H-3″); 3.83 (d, 1H, CH_2 benzyl, J = 16.4 Hz); 4.15 (d, 1H, CH_2 benzyl, J = 16.4 Hz); 5.00 (s, 1H, H-1); 7.12−7.17 (m, 2H, aryl); 7.22 (d, 1H, aryl, J = 7.2 Hz); 7.29 (s, 1NH); 7.36−7.43 (m, 7H, aryl); 7.54 (t, 2H, aryl, J = 8.4 Hz); 7.87 (d, 2H, aryl, J = 8.4 Hz); ^{13}C NMR (100 MHz, $CDCl_3$) δ 20.9; 49.0; 60.3; 63.5; 109.2; 110.8; 118.3; 119.4; 121.7; 127.1; 128.2; 128.4; 128.7; 129.5; 130.0; 133.1; 134.0; 136.1; 136.3; 140.4; 198.1. HR-MS m/z calcd for $C_{25}H_{23}N_2O$ [$(M + H)^+$]: 367.1805; found 367.1812.

*Synthesis of 2-(2-(1H-Indol-3-yl)ethyl)-2,3-dihydro-1H-benzo-[de]isoquinoline (**13**).* One equivalent of 3-(2-bromoethyl)indole was dissolved in acetone, and 1.5 equiv of 2,3-dihydro-1*H*-benzo[de]isoquinoline (**12**), 2.0 equiv of Cs_2CO_3, 1.0 equiv of NaI, and 0.01 equiv of $(CH_3COO)_2Pd$ were added to this solution. The reaction was refluxed for 12 h. The resulting mixture was filtered through Celite, dried in vacuo, and reconstituted in DCM. The organic phase was washed with water (3 × 50 mL), dried over anhydrous Na_2SO_4, filtered, concentrated, and purified by column chromatography using DCM/MeOH as mobile phase.

Colorless oil (69% yield). ^{1}H NMR (400 MHz, $CDCl_3$) δ 2.93 (t, 2H, CH_2, J = 7.6 Hz); 3.10 (t, 2H, CH_2, J = 7.2 Hz); 4.03 (s, 4H, CH_2); 6.97 (s, 1H, aryl); 7.03−7.17 (m, 4H, aryl); 7.26 (d, 1H, aryl, J = 8.0 Hz); 7.33 (t, 2H, aryl, J = 7.2 Hz); 7.57 (d, 1H, aryl, J = 7.6 Hz); 7.63 (d, 2H, aryl, J = 8.0 Hz); 7.92 (s, 1NH); ^{13}C NMR (100 MHz, $CDCl_3$) δ 23.5; 56.9; 58.2; 111.1; 114.3; 119.0; 119.4; 121.7; 122.4; 125.4; 126.5; 127.5; 128.2; 133.2; 133.4; 136.3; 156.6. HR-MS m/z calcd for $C_{22}H_{21}N_2$ [$(M + H)^+$]: 313.1699; found 313.1708.

*General Procedure for the Synthesis of Derivatives **14**−**16**.* *N,N*-Dibenzyl derivatives of L- or D-tryptophan-OMe (**14**, **16**) were obtained by nucleophilic substitution using an excess of (bromomethyl)benzene in the same conditions described for the synthesis of compound **1** and **2**. Starting from **14**, an alkaline hydrolysis of an ester group using NaOH in H_2O/MeOH (4:1 v/v) led to acid compound **15**.

*(S)-Methyl 2-(dibenzylamino)-3-(1H-indol-3-yl)propanoate (**14**).* Colorless oil (75% yield). $[\alpha]^{25}_D$: −21.00 ± 4.83 (c = 0.10, MeOH). ^{1}H NMR (400 MHz, $CDCl_3$); δ 3.14 (dd, 1H, CH_2, J' = 5.6, J'' = 14.4 Hz); 3.44 (dd, 1H, CH_2, J' = 8.8, J'' = 14.0 Hz); 3.60 (d, 2H, CH_2, J = 14.0 Hz); 3.74 (s, 3H, CH_3); 3.87 (dd, 1H, CH, J' = 5.2, J'' = 8.8 Hz); 4.08 (d, 2H, CH_2, J = 13.6 Hz); 6.92 (s, 1H, aryl); 7.00 (t, 1H, aryl, J = 8.0 Hz); 7.16−7.20 (m, 2H, aryl); 7.26−7.39 (m, 11H, aryl); 7.95 (s, 1NH); ^{13}C NMR (100 MHz, $CDCl_3$) δ 26.3; 51.0; 54.7; 61.4; 110.9; 112.1; 118.7; 119.2; 121.8; 122.8; 127.0; 127.5; 128.2; 129.0; 136.2; 139.6; 173.0. HR-MS m/z calcd for $C_{26}H_{27}N_2O_2$ [$(M + H)^+$]: 399.2067; found 399.2073

*(S)-2-(Dibenzylamino)-3-(1H-indol-3-yl)propanoic Acid (**15**).* White solid (58% yield). $[\alpha]^{25}_D$: −35.00 ± 3.98 (c = 0.10, MeOH). ^{1}H NMR (400 MHz, CD_3OD) δ 3.19 (dd, 1H, CH_2, J' = 4.0, J'' = 12.0 Hz); 3.45 (dd, 1H, CH_2, J' = 8.0, J'' = 16.0 Hz); 3.79 (d, 2H, CH_2, J = 12.0 Hz); 3.86 (t, 1H, CH, J = 8.2 Hz); 3.98 (d, 2H, CH_2, J = 12.0); 6.89 (t, 1H, aryl, J = 8.0 Hz); 7.04 (s, 1H, aryl); 7.09 (t, 1H, aryl, J = 8.0 Hz); 7.19 (d, 1H, aryl, J = 8.0 Hz); 7.25−7.30 (m, 10H, aryl); 7.36 (d, 1H, aryl, J = 8.0 Hz); ^{13}C NMR (100 MHz, CD_3OD) δ 25.0; 54.3; 62.2; 110.5; 110.8; 118.0; 118.2; 120.9; 123.1; 127.2; 128.0; 128.8; 136.7; 137.6; 173.6. HR-MS m/z calcd for $C_{25}H_{25}N_2O_2$ [$(M + H)^+$]: 385.1911; found 385.1920

*(R)-Methyl 2-(dibenzylamino)-3-(1H-indol-3-yl)propanoate (**16**).* Colorless oil (71% yield). $[\alpha]^{25}_D$: 27.00 ± 2.12 (c = 0.10, MeOH). ^{1}H NMR (400 MHz, $CDCl_3$): δ 3.14 (dd, 1H, CH_2, J' = 5.6, J'' = 14.4 Hz); 3.44 (dd, 1H, CH_2, J' = 8.8, J'' = 14.0 Hz); 3.60 (d, 2H, CH_2, J = 14.0 Hz); 3.74 (s, 3H, CH_3); 3.87 (dd, 1H, CH, J' = 5.2, J'' = 8.8 Hz); 4.08 (d, 2H, CH_2, J = 13.6 Hz); 6.92 (s, 1H, aryl); 7.00 (t, 1H, aryl, J = 8.0 Hz); 7.16−7.20 (m, 2H, aryl); 7.26−7.39 (m, 11H, aryl); 7.95 (s, 1NH); ^{13}C NMR (100 MHz, $CDCl_3$) δ 26.3; 51.0; 54.7; 61.4; 110.9; 112.1; 118.7; 119.2; 121.8; 122.8; 127.0; 127.5; 128.2; 129.0; 136.2; 139.6; 173.0. HR-MS m/z calcd for $C_{26}H_{27}N_2O_2$ [$(M + H)^+$]: 399.2067; found 399.2073

In Vitro Biological Assays. For fluorescence assays, the HEK293 cells (CRL-1573TM, American Type Culture Collection, LGC Promochem, Molsheim, France) were seeded in 96-well plates (Corning Incorporated, Corning, NY) at a cell density of 40 000 cells 2 days before treatment. On the day of treatment, the medium was replaced with 100 μL of the dye loading solution Fluo-4 NW supplemented with probenecid 2.5 mM. Then the tested molecules dissolved in DMSO were added at the desired concentrations, and the plates were incubated in darkness at 37 °C in a humidified atmosphere of 5% CO_2 for 60 min. The fluorescence was measured using instrument settings appropriate for excitation at 485 nm and emission at 535 nm (POLARstar Omega BMG LABtech). A baseline recording of four cycles was recorded prior to stimulation with the agonist (10 μM capsaicin for TRPV1, 100 μM menthol for TRPM8). Each antagonist (10 μM ruthenium red for TRPV1, 10 μM AMTB for TRPM8) was added to the medium containing the corresponding agonist to induce channel blockade. The changes in fluorescence intensity were recorded during 15 cycles more. The higher

DOI: 10.1021/acs.jmedchem.8b00545
J. Med. Chem. 2018, 61, 6140−6152

concentration of DMSO used in the experiment was added to the control wells. The cells' fluorescence was measured before and after the addition of various concentrations of test compounds (λ_{EX} = 488 nm, λ_{EM} = 516 nm). The fluorescence values obtained are normalized to that prompted by the corresponding agonist (for channel activating compounds) or upon agonist + antagonist coexposure (for channel blocker compounds).

Cell Culture, Transfection, and Whole-Cell Electrophysiology. Most experimental procedures, as well as data processing and analysis, were performed as reported.[30] Briefly, for electrophysiological experiments, HEK293 cells were grown in 100 mm plastic Petri dishes in Dulbecco's modified Eagle's medium containing 10% fetal bovine serum, penicillin (100 U/mL), and streptomycin (100 U/mL) in a humidified atmosphere at 37 °C with 5% CO_2. The cells were seeded in 40 mm dishes containing glass coverslips (Carolina Biological Supply Company, Burlington, NC), which had been previously heat-sterilized and coated with poly-L-lysine to improve cell adhesion. Twenty-four hours after plating, the cells were transiently transfected with a plasmid containing the cDNA encoding the rat isoform of TRPM8 channels (3.6 μg; rTRPM8, a gift from Dr. Felix Viana, Alicante Institute of Neuroscience, Elche, Spain) using Lipofectamine 2000 (Life Technologies, Milan, Italy). A plasmid encoding for the Enhanced Green Fluorescent Protein (EGFP; Clontech, Palo Alto, CA) was used as a transfection marker. Total cDNA in the transfection mixture was kept constant at 4 μg. Twenty-four hours after transfection, patch-clamp recordings in the whole-cell configuration were performed on EGFP-labeled HEK293 cells using an Axopatch 200B amplifier (Molecular Devices, Union City, CA) with glass micropipettes of 3−5 MΩ resistance. The extracellular solution contained (in mM): 138 NaCl, 5.4 KCl, 2 $CaCl_2$, 1 $MgCl_2$, 10 glucose, and 10 HEPES, pH 7.4 with NaOH. The pipet (intracellular) solution contained (in mM): 140 CsCl, 1 EGTA, 10 HEPES, and 5 Mg-ATP, pH 7.3−7.4 with CsOH. The pCLAMP software (version 10.2; Molecular Devices) was used for data acquisition and analysis. Linear cell capacitance (C) was determined by integrating the area under the whole-cell capacity transients, evoked by short (5−10 ms) pulses from −80 to −75 mV with the whole-cell capacitance compensation circuit of the Axopatch 200B turned off. Data were acquired at 5 kHz and filtered at 1−5 kHz with the four-pole low-pass Bessel filter of the amplifier. No correction was made for liquid junction potentials. Currents were evoked by consecutive 100 ms-lasting voltage ramps (from −100 to +100 mV) delivered every 4 s. Currents were measured at +80 or −80 mV and divided by cell capacitance (C) to calculate current densities (expressed in pA/pF).

Homology Modeling. Protein sequence of human TRPM8 was downloaded from the NCBI protein database (NCBI Reference Sequence: NP_076985.4), and the sequence we were interested in, comprising domains S1 to TRP (residues 723−1013), was aligned, using ClustalW,[51] to *Ficedula albicollis* TRPM8 ($TRPM8_{FA}$; PDB ID: 6BPQ).[31] The homology model was built using the energy-based model implemented in Prime,[36a,52] using chain A of $TRPM8_{FA}$ as a template. The obtained model was submitted to the Schrodinger Protein Preparation[53] utility to obtain satisfactory starting structures for the following studies. Optimization of the hydrogen-bonding network was obtained by reorienting hydroxyl and thiol groups, amide groups of Asn and Gln, and His rings. The ionization and tautomeric states of His, Asp, Glu, Arg, and Lys were adjusted to match a pH of 7.4. The structure was finally submitted to a restrained minimization (OPLS2005 force field)[54] that was stopped when rmsd of heavy atoms reached 0.30 Å.

Ligands Preparation. Ligands were sketched using the Maestro[55] interface, and 3D coordinates were generated using LigPrep.[56] Ionization/tautomeric states were predicted for a pH range of 7 ± 1 using Epik.[57]

Molecular Docking. The extended sampling induced fit docking protocol[58] implemented in the Schrödinger Suite was used for the molecular docking simulation of compound **1** to TRPM8. The docking space was defined as a 40 Å cubic boxed centered on the VSLD cavity. The midpoint diameter of ligand was required to lie in a nested 30 Å cubic box. Residues within 5 Å from the ligand atoms were refined, while the rest of the protein was kept fixed. The best scoring **1**/TRPM8 complex was selected for the following studies. Compounds **2**−**4**, **7**−**11**, and **13**−**16** were docked by Glide SP,[39] using the predicted **1**/TRPM8 complex (after 10 ns of MD equilibration) as a target structure. The docking grid was defined as a 40 Å cubic box centered on the induced fit predicted pose of compound **1**, and the ligand diameter midpoint was required to stay in a nested 30 Å cubic box. Receptor OH and SH groups were set free to rotate, and no vdW radii scaling was used for protein atoms, while nonpolar ligand atoms (partial charge less than 0.15) were scaled by a factor of 0.80. Conformational sampling was enhanced by 4 times. The indole ring location was constrained (3 Å) to the position predicted for compound **1**, testing the constrain satisfaction after docking. For each compound only the best scoring solution was retrieved.

Molecular Dynamics Simulations. TRPM8, TRPM8/**1**, and TRPM8/**14** environments were set and run using Desmond MD system;[59] the bound and unbound proteins were inserted into a POPC bilayer, based on the coordinates of the $TRPM8_{FA}$ structure (PDB ID: 6BPQ) from the OPM database.[60] Solvation was treated explicitly, using the TIP4P water model,[61] and OPLS-2005[62] was used as force field. The system was neutralized by Na^+ and Cl^- ions, which were added to a final concentration of 0.15 M. Protein/membrane systems were submitted to the standard equilibration protocol for membrane proteins distributed with Desmond. At this point, 48 ns long MD simulations were carried out at a temperature of 300 K in the isothermal−isobaric ensemble using a Nose−Hoover chain thermostat and a Martyna−Tobias−Klein barostat. Backbone atoms were constrained during the simulation (1 kcal/mol). Trajectory analyses were performed using the Desmond simulation event analysis tool.

In Vivo Assays. C57-mice (males, 5 week old, ∼30 g) (Harlam, Holland) were used for the study. All experiments were approved by the Institutional Animal and Ethical Committee of the Universidad Miguel Hernandez where experiments were conducted, and they were in accordance with the guidelines of the Economic European Community and the Committee for Research and Ethical Issues of the International Association for the Study of Pain. All parts of the study concerning animal care were performed under the control of veterinarians.

WDS Assay. Icilin, a TRPM8 agonist, was dissolved in 20% DMSO and 1% Tween 80 in distilled water and injected intraperitoneally (i.p.) in a volume of 10 mL/kg. Each animal was acclimatized for 30 min for two consecutive days before icilin administration. The compound **14** stock was prepared in DMSO and diluted in saline for injections. Gabapentin was dissolved in saline and administered s.c. at the dose of 25 mg/kg 60 min prior to icillin injection. Control animals received the vehicle injection.

Cold Allodynia. Oxaliplatin (Tocris) was dissolved in water with gentle warming and was subcutaneously (s.c.) injected on days 1, 3, and 5 at a 6 mg/kg dose. The day 7 after administration, experiments were performed. Together with Oxaliplatin injection, saline and a 5% mannitol solution were intraperitoneally injected to prevent kidney damage and dehydration. TRPM8 antagonist stock was prepared in DMSO (Sigma-Aldrich) and diluted in saline for injections. TRPM8 antagonist at different doses (0.1 to 1 μg) was injected into the plantar surface (25 μL) of the right hind paw of mice. Cold chemical thermal sensitivity was assessed using acetone drop method. Mice were placed in a metal mesh cage and allowed to habituate for approximately 30 min in order to acclimatize them. Freshly dispensed acetone drop (10 μL) was applied gently on to the mid plantar surface of the hind paw. Cold chemical sensitive reaction with respect to paw licking was recorded as a positive response (nociceptive pain response). The responses were measured for 20 s with a digital stopwatch. For each measurement, the paw was sampled twice and the mean was calculated. The interval between each application of acetone was approximately 5 min.

Parallel Artificial Membrane Permeability Assay (PAMPA). Donor solution (0.5 mM) was prepared by diluting 10 mM dimethyl

DOI: 10.1021/acs.jmedchem.8b00545
J. Med. Chem. 2018, 61, 6140−6152

sulfoxide (DMSO) compound stock solution using phosphate buffer (pH 7.4, 0.01 M). Filters were coated with 5 μL of a 1% (w/v) dodecane solution of phosphatidylcholine. Donor solution (150 μL) was added to each well of the filter plate. To each well of the acceptor plate was added 300 μL of solution (5% DMSO in phosphate buffer). Derivatives **14** and **15**, propanolol, and furosemide were tested in triplicate. The sandwich was incubated for 24 h at room temperature under gentle shaking. After the incubation time, the sandwich plates were separated, and 300 μL of the acceptor plate was transferred to vial and measured by HPLC with a UV detector at 220 nm. Reference solutions were prepared diluting the sample stock solutions to the same concentration as that with no membrane barrier. The apparent permeability value Papp is determined from the ratio *r* of the absorbance of compound found in the acceptor chamber divided by the theoretical equilibrium absorbance (determined independently) applying the Faller modification of the Sugano equation.[63]

Chemical and Enzymatic Stability Studies. To assess the chemical stability of derivative **14**, a stock solution in DMSO (10 mg/mL) was diluted 1:100 with phosphate buffer and incubated at under stirring at 37 °C. At predetermined intervals (15, 30, and 60 min) the solution was added with dichloromethane (1:1 v:v) and extracted. The organic layer was dried under nitrogen stream, and the residue was reconstituted in 0.9 mL of methanol. After filtration through Phenex nylon syringe filters (0.45 μM, 26 mm, Phenomenex, Castel Maggiore, Italy), the filtrate was analyzed by HPLC. A new HPLC method was set up in order to simultaneously analyze derivatives **14** and **15**, using a Kinetex C18 column (2.6 μM, 100 A, 50 × 2.1 mm, Phenomenex, Castelmaggiore, Italy) and a Shimadzu Nexera HPLC system, consisting of a CBM-20A controller, two LC-20AD pumps, and an SPD-20A detector a SIL-20A HT autosampler (Shimadzu, Kyoto, Japan). The optimal mobile phase consisted of 0.1% CF_3COOH in water v/v (A) and 0.1% CF_3COOH in acetonitrile v/v (B). Separation was performed in gradient elution as follows: 0−7 min, 5−90% B, followed by 3 min of column equilibration. The wavelength used for detection was 220 nm. Flow rate was set at 0.5 mL/min. The analytical system suitability was assessed by checking the linearity range, reproducibility, tailing factor, theoretical plates, and resolution factor. Enzymatic stability studies were carried in mice serum that was kindly gifted by Dr. Rosalinda Sorrentino from the Department of Pharmacy of the University of Salerno. The serum was obtained from retro-orbital mice blood samples using the standard operating procedures. Animal care and manipulations were conducted in conformity with International and National law and policies (EU Directive 2010/63/EU for animal experiments, ARRIVE guidelines, and the Basel declaration including the 3R concept). The stock solution of **14** in DMSO was diluted (1:1000 v/v) with mice serum and incubated at under stirring at 37 °C. The experimental setup used was the same described above for the chemical stability studies. The absence of interfering peaks form serum samples and the efficiency of the extraction method were assessed in bank experiments. All experiments were repeated in triplicate. Preliminary experiments were performed using acetyl salicylic acid as reference compounds to evaluate the hydrolytic activity of mice serum samples.[64]

■ ASSOCIATED CONTENT

Supporting Information

The Supporting Information is available free of charge on the ACS Publications website at DOI: 10.1021/acs.jmedchem.8b00545.

Molecular strings formulas (CSV)

Formatted coordinates of **1** (PDB), **2** (PDB), **3** (PDB), **4** (PDB), **7** (PDB), **8** (PDB), **9** (PDB), **10** (PDB), **11** (PDB), **12** (PDB), **13** (PDB), **14** (PDB), **15** (PDB), and **16** (PDB)

Exemplary HPLC chromatograms of the PAMPA test acceptor solutions; selectivity of compounds **7** and **14** on TRPM8 and TRPV1 channels; similarities between the sequences of interest in human and *Ficedula Albicollis* TRPM8; docking poses of compounds **2**−**4**, **7**−**11**, and **13**; chemical and enzymatic stability graphs for derivatives **14**; metabolic fate of **14** in mice serum; copies of ^{1}H NMR and qDEPT spectra for compounds **2**−**4**, **7**−**11**, and **13**−**15** (PDF)

■ AUTHOR INFORMATION

Corresponding Authors

*(P.C.) Phone: +39-089-969242. E-mail: pcampigl@unisa.it.

*(I.G.-M.) Phone: +39-081-678633. E-mail: imgomez@unina.it.

ORCID

Nunzio Iraci: 0000-0002-1359-8684

Carmine Ostacolo: 0000-0003-3715-8680

Marina Sala: 0000-0003-2739-7215

Ettore Novellino: 0000-0002-2181-2142

Maurizio Taglialatela: 0000-0002-8202-0560

Isabel Gomez-Monterrey: 0000-0001-6688-2606

Author Contributions

#A.B., N. I., and C.O. contributed equally to this work.

Notes

The authors declare no competing financial interest.

■ ACKNOWLEDGMENTS

NVIDIA Corporation is gratefully acknowledged for its support with the donation of the Tesla K40 GPU used for this research. This work has been partially funded by the AEI-MINECO (SAF2015-66275-C2-1) and the GVA (PROMETEO 2014/011).

■ ABBREVIATIONS USED

TRP box, structural motif in the cytosolic C-terminus domain of TRP channel; VSD, voltage sensor domain; VSLD, voltage-sensor-like domain; DCM, dichloromethane; DMF, dimethylformamide; NaH, hydride sodium; THF, tetrahydrofuran; TEA, triethylamine; μW, microwave; TRPV1, transient receptor potential cation channel subfamily V member 1; AITC, allyl isothiocyanate; BCTC, *N*-(4-*tert*-butylphenyl)-4-(3-chloropyridin- 2-yl)piperazine-1-carboxamide; SEM, standard error of the mean; MS, mass spectrometry; ESI, electrospray ionization; MeOH, methanol; DMSO, dimethyl sulfoxide; HEPES, 4-(2-hydroxyethyl)-1-piperazineethanesulfonic acid; EGTA, ethylene glycol tetraacetic acid; POPC, 1-palmitoyl-2-oleoylphosphatidylcholine; rmsd, root-mean-square deviation; MD, molecular dynamics.

■ REFERENCES

(1) McKemy, D. D.; Neuhausser, W. M.; Julius, D. Identification of a cold receptor reveals a general role for TRP channels in thermosensation. *Nature* **2002**, *416*, 52−58.

(2) (a) Peier, A. M.; Moqrich, A.; Hergarden, A. C.; Reeve, A. J.; Andersson, D. A.; Story, G. M.; Earley, T. J.; Dragoni, I.; McIntyre, P.; Bevan, S.; Patapoutian, A. A TRP channel that senses cold stimuli and menthol. *Cell* **2002**, *108*, 705−715. (b) Patapoutian, A.; Peier, A. M.; Story, G. M.; Viswanath, V. ThermoTRP Channels and beyond: mechanisms of temperature sensation. *Nat. Rev. Neurosci.* **2003**, *4*, 529−539.

(3) Babes, A.; Ciobanu, A. C.; Neacsu, C.; Babes, R.-M. TRPM8, a sensor for mild cooling in mammalian sensory nerve endings. *Curr. Pharm. Biotechnol.* **2011**, *12*, 78−88.

DOI: 10.1021/acs.jmedchem.8b00545
J. Med. Chem. 2018, 61, 6140−6152

(4) Kuehn, F. J. P.; Kuehn, C.; Lueckhoff, A. Inhibition of TRPM8 by icilin distinct from desensitization induced by menthol and menthol derivatives. *J. Biol. Chem.* **2009**, *284*, 4102−4111.
(5) (a) Fernandez, J. A.; Skryma, R.; Bidaux, G.; Magleby, K. L.; Scholfield, C. N.; McGeown, J. G.; Prevarskaya, N.; Zholos, A. V. Voltage- and cold-dependent gating of single TRPM8 ion channels. *J. Gen. Physiol.* **2011**, *137*, 173−195. (b) Raddatz, N.; Castillo, J. P.; Gonzalez, C.; Alvarez, O.; Latorre, R. Temperature and voltage coupling to channel opening in transient receptor potential melastatin 8 (TRPM8). *J. Biol. Chem.* **2014**, *289*, 35438−35454.
(6) (a) Rohács, T.; Lopes, C. M.; Michailidis, I.; Logothetis, D. E. PI(4,5)P2 regulates the activation and desensitization of TRPM8 channels through the TRP domain. *Nat. Neurosci.* **2005**, *8*, 626−634. (b) Liu, B.; Qin, F. Functional control of cold- and menthol-sensitive TRPM8 ion channels by phosphatidylinositol 4,5-bisphosphate. *J. Neurosci.* **2005**, *25*, 1674−1681.
(7) Liu, Y.; Qin, N. TRPM8 in health and disease: cold sensing and beyond. *Adv. Exp. Med. Biol.* **2011**, *704*, 185−208.
(8) McKemy, D. D. Therapeutic potential of TRPM8 modulators. *Open Drug Discovery J.* **2010**, *2*, 81−88.
(9) Journigan, V. B.; Zaveri, N. T. TRPM8 ion channel ligands for new therapeutic applications and as probes to study menthol pharmacology. *Life Sci.* **2013**, *92*, 425−437.
(10) (a) Parra, A.; Madrid, R.; Echevarria, D.; del Olmo, S.; Morenilla- Palao, C.; Acosta, C. M.; Gallar, J.; Dhaka, A.; Viana, F.; Belmonte, C. Ocular surface wetness is regulated by TRPM8-dependent cold thermoreceptors of the cornea. *Nat. Med.* **2010**, *16*, 1396−1399. (b) Dhaka, A.; Earley, T. J.; Watson, J.; Patapoutian, A. Visualizing cold spots: TRPM8-expressing sensory neurons and their projections. *J. Neurosci.* **2008**, *28*, 566−575.
(11) De Blas, G. A.; Darszon, A.; Ocampo, A. Y.; Serrano, C. J.; Castellano, L. E.; Hernandez-Gonzalez, E. O.; Chirinos, M.; Larrea, F.; Beltran, C.; Trevino, C. L. TRPM8, a versatile channel in human sperm. *PLoS One* **2009**, *4*, e6095.
(12) Sabnis, A. S.; Shadid, M.; Yost, G. S.; Reilly, C. A. Human lung epithelial cells express a functional cold-sensing TRPM8 variant. *Am. J. Respir. Cell Mol. Biol.* **2008**, *39*, 466−474.
(13) Johnson, C. D.; Melanaphy, D.; Purse, A.; Stokesberry, S. A.; Dickson, P.; Zholos, A. V. Transient receptor potential melastatin 8 channel involvement in the regulation of vascular tone. *Am. J. Physiol. Heart Circ. Physiol* **2009**, *296*, H1868−1877.
(14) (a) Chuang, H. H.; Neuhausser, W. M.; Julius, D. The super-cooling agent icilin reveals a mechanism of coincidence detection by a temperature-sensitive TRP channel. *Neuron* **2004**, *43*, 859−869. (b) Xing, H.; Chen, M.; Ling, J.; Tan, W.; Gu, J. G. TRPM8 mechanism of cold allodynia after chronic nerve injury. *J. Neurosci.* **2007**, *27*, 13680−13690.
(15) Proudfoot, C. J.; Garry, E. M.; Cottrell, D. F.; Rosie, R.; Anderson, H.; Robertson, D. C.; Fleetwood-Walker, S. M.; Mitchell, R. Analgesia mediated by the TRPM8 cold receptor in chronic neuropathic pain. *Curr. Biol.* **2006**, *16*, 1591−1605.
(16) Bautista, D. M.; Siemens, J.; Glazer, J. M.; Tsuruda, P. R.; Basbaum, A. I.; Stucky, C. L.; Jordt, S. E.; Julius, D. The menthol receptor TRPM8 is the principal detector of environmental cold. *Nature* **2007**, *448*, 204−208.
(17) Knowlton, W. M.; Daniels, R. L.; Palkar, R.; McCoy, D. D.; McKemy, D. D. Pharmacological blockade of TRPM8 ion channels alters cold and cold pain responses in mice. *PLoS One* **2011**, *6*, e25894.
(18) (a) Tsavaler, L.; Shapero, M. H.; Morkowski, S.; Laus, R. Trp-p8, a novel prostate-specific gene, is up-regulated in prostate cancer and other malignancies and shares high homology with transient receptor potential calcium channel proteins. *Cancer Res.* **2001**, *61*, 3760−3769. (b) Zhang, L.; Barritt, G. J. Evidence that TRPM8 is an androgendependent Ca2+ channel required for the survival of prostate cancer cells. *Cancer Res.* **2004**, *64*, 8365−8373.
(19) (a) Yamamura, H.; Ugawa, S.; Ueda, T.; Morita, A.; Shimada, S. TRPM8 activation suppresses cellular viability in human melanoma. *Am. J. Physiol. Cell Physiol.* **2008**, *295*, C296−301. (b) Dhennin-Duthille, I.; Gautier, M.; Faouzi, M.; Guilbert, A.; Brevet, M.; Vaudry, D.; Ahidouch, A.; Sevestre, H.; Ouadid-Ahidouch, H. High expression of transient receptor potential channels in human breast cancer epithelial cells and tissues: correlation with pathological parameters. *Cell. Physiol. Biochem.* **2011**, *28*, 813−822. (c) Yee, N. S.; Zhou, W.; Lee, M. Transient receptor potential channel TRPM8 is over-expressed and required for cellular proliferation in pancreatic adenocarcinoma. *Cancer Lett.* **2010**, *297*, 49−55.
(20) Moran, M. M.; McAlexander, M. A.; Biro, T.; Szallasi, A. Transient receptor potential channels as therapeutic targets. *Nat. Rev. Drug Discovery* **2011**, *10*, 601−620.
(21) Malkia, A.; Morenilla-Palao, C.; Viana, F. The emerging pharmacology of TRPM8 channels: hidden therapeutic potential underneath a cold surface. *Curr. Pharm. Biotechnol.* **2011**, *12*, 54−67.
(22) Knowlton, W. M.; McKemy, D. D. TRPM8: from cold to cancer, peppermint to pain. *Curr. Pharm. Biotechnol.* **2011**, *12*, 68−77.
(23) Vay, L.; Gu, C.; McNaughton, P. A. The thermo-TRP ion channel family: properties and therapeutic implications. *Br. J. Pharmacol.* **2012**, *165*, 787−801.
(24) (a) Ferrer-Montiel, A.; Fernandez-Carvajal, A.; Planells-Cases, R.; Fernandez-Ballester, G.; Gonzalez-Ros, J. M.; Messeguer, A.; Gonzalez-Muniz, R. Advances in modulating thermosensory TRP channels. *Expert Opin. Ther. Pat.* **2012**, *22*, 999−1017. (b) Pérez de Vega, M. J.; Gómez-Monterrey, I.; Ferrer-Montiel, A.; González-Muñiz, R. Transient receptor potential melastatin 8 channel (TRPM8) modulation: cool entryway for treating pain and cancer. *J. Med. Chem.* **2016**, *59*, 10006−10029 and references therein.
(25) Holzer, P.; Izzo, A. A. The pharmacology of TRP channels. *Br. J. Pharmacol.* **2014**, *171*, 2469−2473.
(26) (a) Madrid, R.; Donovan-Rodríguez, T.; Meseguer, V.; Acosta, M. C.; Belmonte, C.; Viana, F. Contribution of TRPM8 channels to cold transduction in primary sensory neurons and peripheral nerve terminals. *J. Neurosci.* **2006**, *26*, 12512−12525. (b) Valero, M.; Morenilla-Palao, C.; Belmonte, C.; Viana, F. Pharmacological and functional properties of TRPM8 channels in prostate tumor cells. *Pfluegers Arch.* **2011**, *461*, 99−114.
(27) Lashinger, E. S.; Steiginga, M. S.; Hieble, J. P.; Leon, L. A.; Gardner, S. D.; Nagilla, R.; Davenport, E. A.; Hoffman, B. E.; Laping, N. J.; Su, X. AMTB, a TRPM8 channel blocker: evidence in rats for activity in overactive bladder and painful bladder syndrome. *Am. J. Physiol. Renal Physiol.* **2008**, *295*, F803−810.
(28) Parks, D. J.; Parsons, W. H.; Colburn, R. W.; Meegalla, S. K.; Ballentine, S. K.; Illig, C. R.; Qin, N.; Liu, Y.; Hutchinson, T. L.; Lubin, M. L.; Stone, D. J., Jr.; Baker, J. F.; Schneider, C. R.; Ma, J.; Damiano, B. P.; Flores, C. M.; Player, M. R. Design and optimization of benzimidazole-containing transient receptor potential melastatin 8 (TRPM8) antagonists. *J. Med. Chem.* **2011**, *54*, 233−247.
(29) (a) Winchester, W. J.; Gore, K.; Glatt, S.; Petit, W.; Gardiner, J. C.; Conlon, K.; Postlethwaite, M.; Saintot, P. P.; Roberts, S.; Gosset, J. R.; Matsuura, T.; Andrews, M. D.; Glossop, P. A.; Palmer, M. J.; Clear, N.; Collins, S.; Beaumont, K.; Reynolds, D. S. Inhibition of TRPM8 channels reduces pain in the cold pressor test in humans. *J. Pharmacol. Exp. Ther.* **2014**, *351*, 259−269. (b) Andrews, M. D.; Af Forselles, K.; Beaumont, K.; Galan, S. R.; Glossop, P. A.; Grenie, M.; Jessiman, A.; Kenyon, A. S.; Lunn, G.; Maw, G.; Owen, R. M.; Pryde, D. C.; Roberts, D.; Tran, T. D. Discovery of a selective TRPM8 antagonist with clinical efficacy in cold-related pain. *ACS Med. Chem. Lett.* **2015**, *6*, 419−424.
(30) Bertamino, A.; Ostacolo, C.; Ambrosino, P.; Musella, S.; Di Sarno, V.; Ciaglia, T.; Soldovieri, M. V.; Iraci, N.; Fernández Carvajal, A.; de la Torre-Martínez, R.; Ferrer-Montiel, A.; González Muniz, R.; Novellino, E.; Taglialatela, M.; Campiglia, P.; Gómez-Monterrey, I. Tryptamine based derivatives as transient receptor potential melastatin type 8 (TRPM8) channel modulators. *J. Med. Chem.* **2016**, *59*, 2179−2191.
(31) Yin, Y.; Wu, M.; Zubcevic, L.; Borschel, W. F.; Lander, G. C.; Lee, S.-Y. Structure of the cold- and menthol-sensing ion channel TRPM8. *Science* **2018**, *359*, 237−241.

DOI: 10.1021/acs.jmedchem.8b00545
J. Med. Chem. 2018, 61, 6140−6152

(32) Taberner, F. J.; López-Córdoba, A.; Fernández-Ballester, G.; Korchev, Y.; Ferrer-Montiel, A. The region adjacent to the C-end of the inner gate in transient receptor potential melastatin 8 (TRPM8) channels plays a central role in allosteric channel activation. *J. Biol. Chem.* **2014**, *289*, 28579−28594.
(33) De la Torre-Martínez, R.; Bonache, M. A.; Llabrés-Campaner, P. J.; Balsera, B.; Fernández-Carvajal, A.; Fernández-Ballester, G.; Ferrer-Montiel, A.; Pérez de Vega, M. J.; González-Muñiz, R. Synthesis, high-throughput screening and pharmacological characterization of β−lactam derivatives as TRPM8 antagonists. *Sci. Rep.* **2017**, *7*, 10766.
(34) Beccari, A. R.; Gemei, M.; Monte, M. L.; Menegatti, N.; Fanton, M.; Pedretti, A.; Bovolenta, S.; Nucci, C.; Molteni, A.; Rossignoli, A.; Brandolini, L.; Taddei, A.; Za, L.; Liberati, C.; Vistoli, G. Novel selective, potent naphthyl TRPM8 antagonists identified through a combined ligand- and structure-based virtual screening approach. *Sci. Rep.* **2017**, *7*, 10999.
(35) De Petrocellis, L.; Arroyo, F. J.; Orlando, P.; Schiano Moriello, A.; Vitale, R. M.; Amodeo, P.; Sánchez, A.; Roncero, C.; Bianchini, G.; Martín, M. A.; López-Alvarado, P.; Menéndez, J. C. Tetrahydroisoquinoline-derived urea and 2,5-diketopiperazine derivatives as selective antagonists of the transient receptor potential melastatin 8 (TRPM8) channel receptor and antiprostate cancer agents. *J. Med. Chem.* **2016**, *59*, 5661−5683.
(36) (a) Jacobson, M. P.; Pincus, D. L.; Rapp, C. S.; Day, T. J. F.; Honig, B.; Shaw, D. E.; Friesner, R. A. A Hierarchical Approach to all-atom protein loop prediction. *Proteins: Struct., Funct., Genet.* **2004**, *55*, 351−367. (b) Jacobson, M. P.; Friesner, R. A.; Xiang, Z.; Honig, B. On the role of crystal packing forces in determining protein sidechain conformations. *J. Mol. Biol.* **2002**, *320*, 597−608.
(37) Farid, R.; Day, T.; Friesner, R. A.; Pearlstein, R. A. New insights about HERG blockade obtained from protein modeling, potential energy mapping, and docking studies. *Bioorg. Med. Chem.* **2006**, *14*, 3160−3173.
(38) (a) Sherman, W.; Day, T.; Jacobson, M. P.; Friesner, R. A.; Farid, R. Novel procedure for modeling ligand/receptor induced fit effects. *J. Med. Chem.* **2006**, *49*, 534−553. (b) Sherman, W.; Beard, H. S.; Farid, R. Use of an induced fit receptor structure in virtual screening. *Chem. Biol. Drug Des.* **2006**, *67*, 83−84.
(39) Friesner, R. A.; Banks, J. L.; Murphy, R. B.; Halgren, T. A.; Klicic, J. J.; Mainz, D. T.; Repasky, M. P.; Knoll, E. H.; Shaw, D. E.; Shelley, M.; Perry, J. K.; Francis, P.; Shenkin, P. S. Glide: a new approach for rapid, accurate docking and scoring. 1. Method and assessment of docking accuracy. *J. Med. Chem.* **2004**, *47*, 1739−1749.
(40) Malkia, T. O.; Pertusa, M.; Fernández-Ballester, G.; Ferrer-Montiel, A.; Viana, F. Differential role of the menthol-binding residue Y745 in the antagonism of thermally gated TRPM8 channels. *Mol. Pain* **2009**, *5*, 62.
(41) (a) Wei, E. T. Inhibition of shaking movements in rats by central administration of cholinergic and adrenergic agents. *Psychopharmacology (Berl)* **1983**, *81*, 111−114. (b) Wei, E. T.; Seid, D. A. AG-3−5: a chemical producing sensations of cold. *J. Pharm. Pharmacol.* **1983**, *35*, 110−112.
(42) (a) Colburn, R. W.; Lubin, M. L.; Stone, D. J., Jr; Wang, Y.; Lawrence, D.; D'Andrea, M. R.; Brandt, M. R.; Liu, Y.; Flores, C. M.; Qin, N. Attenuated cold sensitivity in TRPM8 null mice. *Neuron* **2007**, *54*, 379−386. (b) Dhaka, A.; Murray, A. N.; Mathur, J.; Earley, T. J.; Petrus, M. J.; Patapoutian, A. TRPM8 is required for cold sensation in mice. *Neuron* **2007**, *54*, 371−378.
(43) Kono, T.; Satomi, M.; Suno, M.; Kimura, N.; Yamazaki, H.; Furukawa, H.; Matsubara, K. Oxaliplatin-induced neurotoxicity involves TRPM8 in the mechanism of acute hypersensitivity to cold sensation. *Brain Behav* **2012**, *2*, 68−73.
(44) (a) Ling, B.; Authier, N.; Balayssac, D.; Eschalier, A.; Coudore, F. Behavioral and pharmacological description of oxaliplatin-induced painful neuropathy in rat. *Pain* **2007**, *128*, 225−234. (b) Ling, B.; Coudore-Civiale, M. A.; Balayssac, D.; Eschalier, A.; Coudore, F.; Authier, N. Behavioral and immunohistological assessment of painful neuropathy induced by a single oxaliplatin injection in the rat. *Toxicology* **2007**, *234*, 176−184.
(45) Authier, N.; Balayssac, D.; Marchand, F.; Ling, B.; Zangarelli, A.; Descoeur, J.; Coudore, F.; Bourinet, E.; Eschalier, A. Animal models of chemotherapy-evoked painful peripheral neuropathies. *Neurotherapeutics* **2009**, *6*, 620−629.
(46) Patel, R.; Gonçalves, L.; Leveridge, M.; Mack, S. R.; Hendrick, A.; Brice, N. L.; Dickenson, A. H. Anti-hyperalgesic effects of a novel TRPM8 agonist in neuropathic rats: a comparison with topical menthol. *Pain* **2014**, *155*, 2097−2107.
(47) Fallon, M. T.; Storey, D. J.; Krishan, A.; Weir, C. J.; Mitchell, R.; Fleetwood-Walker, S. M.; Scott, A. C.; Colvin, L. A. Cancer treatment-related neuropathic pain: proof of concept study with menthol—a TRPM8 agonis. *Support. Care Cancer* **2015**, *23*, 2769−2777. (b) Storey, D. J.; Colvin, L. A.; Mackean, M. J.; Mitchell, R.; Fleetwood-Walker, S. M.; Fallon, M. T. Reversal of dose-limiting carboplatin-induced peripheral neuropathy with TRPM8 activator, menthol, enables further effective chemotherpy delivery. *J. Pain Symptom Manage.* **2010**, *39*, e2−4.
(48) (a) Gauchan, P.; Andoh, T.; Kato, A.; Kuraishi, Y. Involvement of increased expression of transient receptor potential melastatin 8 in oxaliplatin-induced cold allodynia in mice. *Neurosci. Lett.* **2009**, *458*, 93−95. (b) Mizoguchi, S.; Andoh, T.; Yakura, T.; Kuraishi, Y. Involvement of c-Myc-mediated transient receptor potential melastatin 8 expression in oxaliplatin-induced cold allodynia in mice. *Pharmacol. Rep.* **2016**, *68*, 645−648.
(49) (a) Binder, A.; Stengel, M.; Maag, R.; Wasner, G.; Schoch, R.; Moosig, F.; Schommer, B.; Baron, R. Pain in oxaliplatin-induced neuropathy − sensitisation in the peripheral and central nociceptive system. *Eur. J. Cancer* **2007**, *43*, 2658−2663. (b) Zhao, M.; Isami, K.; Nakamura, S.; Shirakawa, H.; Nakagawa, T.; Kaneko, S. Acute cold hypersensitivity characteristically induced by oxaliplatin is caused by the enhanced responsiveness of TRPA1 in mice. *Mol. Pain* **2012**, *8*, 55. (c) Nassini, R.; Gees, M.; Harrison, S.; De Siena, G.; Materazzi, S.; Moretto, N.; Failli, P.; Preti, D.; Marchetti, N.; Cavazzini, A.; Mancini, F.; Pedretti, P.; Nilius, B.; Patacchini, R.; Geppetti, P. Oxaliplatin elicits mechanical and cold allodynia in rodents via TRPA1 receptor stimulation. *Pain* **2011**, *152*, 1621−1631.
(50) Pan, Y.; Chen, F.; Huang, S.; Cai, Z.; Lan, H.; Tong, Y.; Yu, X.; Zhao, G. TRPA1 and TRPM8 receptors may promote local vasodilation that aggravates oxaliplatin-induced peripheral neuropathy amenable to 17β-estradiol treatment. *Curr. Neurovasc Res.* **2016**, *13*, 309−317.
(51) Thompson, J. D.; Higgins, D. G.; Gibson, T. J. CLUSTAL W: improving the sensitivity of progressive multiple sequence alignment through sequence weighting, position-specific gap penalties and weight matrix choice. *Nucleic Acids Res.* **1994**, *22* (22), 4673−4680.
(52) (b) Jacobson, M. P.; Friesner, R. A.; Xiang, Z.; Honig, B. On the role of crystal packing forces in determining protein sidechain conformations. *J. Mol. Biol.* **2002**, *320*, 597−608.
(53) Madhavi Sastry, G.; Adzhigirey, M.; Day, T.; Annabhimoju, R.; Sherman, W. Protein and ligand preparation: parameters, protocols, and influence on virtual screening enrichments. *J. Comput.-Aided Mol. Des.* **2013**, *27* (3), 221−234.
(54) Jorgensen, W. L.; Maxwell, D. S.; Tirado-Rives, J. Development and testing of the OPLS all atom force field on conformational energetics and properties of organic liquids. *J. Am. Chem. Soc.* **1996**, *118*, 11225−11236.
(55) *Maestro*; Schrödinger LLC: New York, 2017.
(56) *LigPrep*; Schrödinger, LLC: New York, 2017.
(57) (a) Greenwood, J. R.; Calkins, D.; Sullivan, A. P.; Shelley, J. C. Towards the comprehensive, rapid, and accurate prediction of the favorable tautomeric states of drug-like molecules in aqueous solution. *J. Comput.-Aided Mol. Des.* **2010**, *24*, 591−604. (b) Shelley, J. C.; Cholleti, A.; Frye, L.; Greenwood, J. R.; Timlin, M. R.; Uchimaya, M. Epik: a software program for pKa prediction and protonation state generation for drug-like molecules. *J. Comput.-Aided Mol. Des.* **2007**, *21*, 681−691.

DOI: 10.1021/acs.jmedchem.8b00545
J. Med. Chem. 2018, 61, 6140−6152

(58) (a) Sherman, W.; Day, T.; Jacobson, M. P.; Friesner, R. A.; Farid, R. Novel procedure for modeling ligand/receptor induced fit effects. *J. Med. Chem.* **2006**, *49*, 534−553. (b) Sherman, W.; Beard, H. S.; Farid, R. Use of an induced fit receptor structure in virtual screening. *Chem. Biol. Drug Des.* **2006**, *67*, 83−84.

(59) (a) *Desmond Molecular Dynamics System*; DE Shaw Research: New York, 2015. (b) *Maestro-Desmond Interoperability Tools*; Schrödinger LLC: New York, 2015. (c) Bowers, K. J.; Chow, E.; Xu, H.; Dror, R. O.; Eastwood, M. P.; Gregersen, B. A.; Klepeis, J. L.; Kolossvary, I.; Moraes, M. A.; Sacerdoti, F. D.; Salmon, J. K.; Shan, Y.; Shaw, D. E. Scalable algorithms for molecular dynamics simulations on commodity clusters. In *Proceedings of ACM/IEEE Supercomputing Conference*, ACM/IEEE, November 11−14 2006; Tampa, FL, 2006; DOI: 10.1109/SC.2006.54.

(60) Lomize, M. A.; Lomize, A. L.; Pogozheva, I. D.; Mosberg, H. I. OPM: orientations of proteins in membranes database. *Bioinformatics* **2006**, *22* (5), 623−625.

(61) Jorgensen, W. L.; Chandrasekhar, J.; Madura, J. D.; Impey, R. W.; Klein, M. L. Comparison of simple potential functions for simulating liquid water. *J. Chem. Phys.* **1983**, *79*, 926−935.

(62) Jorgensen, W. L.; Maxwell, D. S.; Tirado-Rives, J. Development and testing of the OPLS all atom force field on conformational energetics and properties of organic liquids. *J. Am. Chem. Soc.* **1996**, *118*, 11225−11236.

(63) Wohnsland, F.; Faller, B. High-throughput permeability pH profile and high-throughput alkane/water log P with artificial membranes. *J. Med. Chem.* **2001**, *44*, 923−930.

(64) Marra, F.; Ostacolo, C.; Laneri, S.; Bernardi, A.; Sacchi, A.; Padula, C.; Nicoli, S.; Santi, P. Synthesis, hydrolysis, and skin retention of amino acid esters of alpha-tocopherol. *J. Pharm. Sci.* **2009**, *98*, 2364−2376.

DOI: 10.1021/acs.jmedchem.8b00545
J. Med. Chem. 2018, 61, 6140−6152